UNIVERSITY OF MICHIGAN

VOLUME 33 JULY 1955 NUMBER 4 ENGINEERING LIBRARY

Canadian Journal of Technology

Editor: G. A. LEDINGHAM

Published by THE NATIONAL RESEARCH COUNCIL
OTTAWA CANADA

CANADIAN JOURNAL OF TECHNOLOGY

(Formerly Section F, Canadian Journal of Research)

Under the authority of the Chairman of the Committee of the Privy Council on Scientific and Industrial Research, the National Research Council issues THE CANADIAN JOURNAL OF TECHNOLOGY and six other journals devoted to the publication, in English or French, of the results of original scientific research. Matters of general policy concerning these journals are the responsibility of a joint Editorial Board consisting of: members representing the National Research Council of Canada; the Editors of the Journals; and members representing the Royal Society of Canada and four other scientific societies.

The Chemical Institute of Canada has chosen the Canadian Journal of Technology and the Canadian Journal of Chemistry as its medium of publication for scientific papers.

EDITORIAL BOARD

Representatives of the National Research Council

A. N. Campbell, *University of Manitoba*
G. E. Hall, *University of Western Ontario*
E. G. D. Murray, *McGill University*
D. L. Thomson, *McGill University*
W. H. Watson (Chairman), *University of Toronto*

Editors of the Journals

D. L. Bailey, *University of Toronto*
J. B. Collip, *University of Western Ontario*
E. H. Craigie, *University of Toronto*
G. A. Ledingham, *National Research Council*
Léo Marion, *National Research Council*
R. G. E. Murray, *University of Western Ontario*
G. M. Volkoff, *University of British Columbia*

Representatives of Societies

D. L. Bailey, *University of Toronto*
Royal Society of Canada
J. B. Collip, *University of Western Ontario*
Canadian Physiological Society
E. H. Craigie, *University of Toronto*
Royal Society of Canada
R. G. E. Murray, *University of Western Ontario*
Canadian Society of Microbiologists
H. G. Thode, *McMaster University*
Chemical Institute of Canada
T. Thorvaldson, *University of Saskatchewan*
Royal Society of Canada
G. M. Volkoff, *University of British Columbia*
Royal Society of Canada; Canadian Association of Physicists

Ex officio

Léo Marion (Editor-in-Chief), *National Research Council*

Manuscripts for publication should be submitted to Dr. Léo Marion, Editor-in-Chief, Canadian Journal of Technology, National Research Council, Ottawa 2, Canada.
(For instructions on preparation of copy, see **Notes to Contributors** (inside back cover).)

Proof, correspondence concerning proof, and orders for reprints should be sent to the Manager, Editorial Office (Research Journals), Division of Administration, National Research Council, Ottawa 2, Canada.

Subscriptions, renewals, requests for single or back numbers, and all remittances should be sent to Division of Administration, National Research Council, Ottawa 2, Canada. Remittances should be made payable to the Receiver General of Canada, credit National Research Council.

The journals published, frequency of publication, and prices are:

Canadian Journal of Biochemistry and Physiology	Bimonthly	$3.00 a year
Canadian Journal of Botany	Bimonthly	$4.00 a year
Canadian Journal of Chemistry	Monthly	$5.00 a year
Canadian Journal of Microbiology*	Bimonthly	$3.00 a year
Canadian Journal of Physics	Monthly	$4.00 a year
Canadian Journal of Technology	Bimonthly	$3.00 a year
Canadian Journal of Zoology	Bimonthly	$3.00 a year

The price of single numbers of all journals is 75 cents.

*Volume 1 will combine three numbers published in 1954 with six published in 1955 and will be available at the regular annual subscription rate of $3.00.

Contents

Page

Plastic Deformations Due to Dynamic Loading of a Beam with an Attached Mass—*T. J. Mentel* - - - - - - - - - - 237

Some Characteristics of Spray-dried Wheat Gluten—*W. B. McConnell* - - - - - - - - - - - - - - - - 256

Humidification of Cold Storages: The Jacket System—*C. P. Lentz* 265

Automatic Translation of Aeration Data Between Different Fermentors—*Ping Shu* - - - - - - - - - - - 279

The Storage and Transfer of Low Potential Heat. I. Glauber's Salt as a Heat Storage Material—*J. W. Hodgins and T. W. Hoffman* 293

An Operation-time Controller for a Recording Potentiometer—*G. O. Handegord and D. G. Cole* - - - - - - - - - 303

Printed in Canada *by* University of Toronto Press

CANADIAN JOURNAL OF TECHNOLOGY

Notes to Contributors

Manuscripts

(i) ***General.*** Manuscripts, in English or French, should be typewritten, double spaced, on paper 8½×11 in. **The original and one copy are to be submitted.** Tables and captions for the figures should be placed at the end of the manuscript. Every sheet of the manuscript should be numbered.

Style, arrangement, spelling, and abbreviations should conform to the usage of this journal. Names of all simple compounds, rather than their formulas, should be used in the text. Greek letters or unusual signs should be written plainly or explained by marginal notes. Superscripts and subscripts must be legible and carefully placed.

Manuscripts should be carefully checked before they are submitted; authors will be charged for changes made in the proof that are considered excessive.

(ii) ***Abstract.*** An abstract of not more than about 200 words, indicating the scope of the work and the principal findings, is required, except in Notes.

(iii) ***References.*** References should be listed **alphabetically by authors' names,** numbered, and typed after the text. The form of the citations should be that used in this journal; in references to papers in periodicals, inclusive page numbers should be given but titles should not. All citations should be checked with the original articles and each one referred to in the text by the key number.

(iv) ***Tables.*** Tables should be numbered in roman numerals and each table referred to in the text. Titles should always be given but should be brief; column headings should be brief and descriptive matter in the tables confined to a minimum. Vertical rules should be used only when they are essential. Numerous small tables should be avoided.

Illustrations

(i) ***General.*** All figures (including each figure of the plates) should be numbered consecutively from 1 up, in arabic numerals, and each figure referred to in the text. The author's name, title of the paper, and figure number should be written in the lower left corner of the sheets on which the illustrations appear. Captions should not be written on the illustrations (see Manuscripts (i)).

(ii) ***Line Drawings.*** Drawings should be carefully made with India ink on white drawing paper, blue tracing linen, or co-ordinate paper ruled in blue only; any co-ordinate lines that are to appear in the reproduction should be ruled in black ink. Paper ruled in green, yellow, or red should not be used unless it is desired to have all the co-ordinate lines show. All lines should be of sufficient thickness to reproduce well. Decimal points, periods, and stippled dots should be solid black circles large enough to be reduced if necessary. Letters and numerals should be neatly made, preferably with a stencil (**do NOT use typewriting**) and be of such size that the smallest lettering will be not less than 1 mm. high when reproduced in a cut 3 in. wide.

Many drawings are made too large; originals should not be more than 2 or 3 times the size of the desired reproduction. In large drawings or groups of drawings the ratio of height to width should conform to that of a journal page but the height should be adjusted to make allowance for the caption.

The original drawings and one set of clear copies (e.g. small photographs) are to be submitted.

(iii) ***Photographs.*** Prints should be made on glossy paper, with strong contrasts. They should be trimmed so that essential features only are shown and mounted carefully, with rubber cement, on white cardboard with no space or only a very small space (less than 1 mm.) between them. In mounting, full use of the space available should be made (to reduce the number of cuts required) and the ratio of height to width should correspond to that of a Journal page (4½×7½ in.); however, allowance must be made for the captions. Photographs or groups of photographs should not be more than 2 or 3 times the size of the desired reproduction.

Photographs are to be submitted in duplicate; if they are to be reproduced in groups one set should be mounted, the duplicate set unmounted.

Reprints

A total of 50 reprints of each paper, without covers, are supplied free. Additional reprints, with or without covers, may be purchased.

Charges for reprints are based on the number of printed pages, which may be calculated approximately by multiplying by 0.6 the number of manuscript pages (double-spaced typewritten sheets, 8½×11 in.) and including the space occupied by illustrations. An additional charge is made for illustrations that appear as coated inserts. The cost per page is given on the reprint requisition which accompanies the galley.

Any reprints required in addition to those requested on the author's reprint requisition form must be ordered officially as soon as the paper has been accepted for publication.

Canadian Journal of Technology

Issued by THE NATIONAL RESEARCH COUNCIL OF CANADA

VOLUME 33 JULY 1955 NUMBER 4

PLASTIC DEFORMATIONS DUE TO DYNAMIC LOADING OF A BEAM WITH AN ATTACHED MASS[1]

BY T. J. MENTEL[2]

ABSTRACT

The influence of an attached mass on the large plastic deformations of a beam subjected to dynamic pressure loading is examined. The particular cases worked out in detail are those of a simply supported and a built-in beam, subjected to a uniform pressure pulse of a rectangular shape. In the analysis elastic strains are assumed to be negligible. The results contrast with those of the uniform beam in certain respects. The successive configurations of deformation excited by loads of various magnitudes are more complex than in the uniform beam (zero attached mass) case. Moreover, a new phenomenon appears, namely that plastic strains in the beam adjacent to the attached mass take place first in one direction and subsequently in the opposite sense, when the load magnitude exceeds a certain value. This reversal of sign of plastic flow may be important from the point of view of rupture, although the general effect of the attached mass is to strongly reduce the magnitude of the deflections of the beam. A discussion of the limitations and possible accuracy of an approximate solution based on a simple one-dimensional model is included.

INTRODUCTION

The primary purpose of this investigation is to study the effect of a mass attached to a beam (Fig. 1) on the deformations produced by dynamic pressure loading. The results are also applicable at once to the case of a portal frame (Fig. 2) in which the horizontal member is assumed to be rigid and to have negligible depth, and in which the load is assumed to be applied equally to both columns.

The so-called plastic-rigid type of analysis, which is used in this paper, has already been applied to several problems of uniform beams involving various end conditions and types of dynamic loading (3, 4). The basic assumptions of this method, as applied to transverse deformations of beams, can be summarized as follows:

(i) Only plastic flexural deformation is significant, and this occurs only when the moment at any cross-section reaches and maintains a fixed magnitude M_0, termed the "limit moment" of the beam section.

(ii) "Plastic hinges" occur at all sections where M_0 is maintained. When the value M_0 is maintained at a given cross-section of the beam, the plastic hinge

[1]*Manuscript received February 1, 1955.*

Contribution from the Division of Applied Mathematics, Brown University, Providence, Rhode Island, U.S.A. The results presented in this paper were obtained in the course of research sponsored by Norfolk Naval Shipyard under Contract N189s–92558.

[2]*Research Assistant in the Graduate Division of Applied Mathematics, Brown University.*

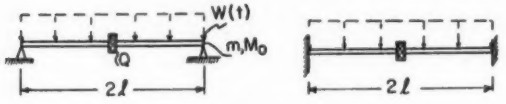

Fig. 1

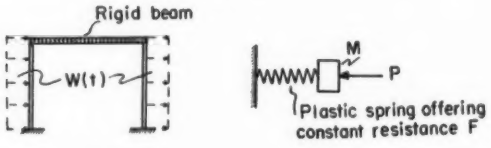

Fig. 2 Fig. 3

FIG. 1. Beams analyzed in paper.
FIG. 2. Equivalent portal frame.
FIG. 3. One-dimensional model.

allows a discontinuity in the slope of the beam to occur across this section. If the moment has magnitude M_0 over a finite distance, the plastic "hinge" becomes a finite plastic zone.

(iii) Shear and axial forces occurring at plastic hinges are not large enough to have an appreciable effect on the value of M_0.

(iv) All displacements are assumed small so that changes in beam geometry can be neglected in setting up the equations.

This concept of localization of deformation at plastic hinges has led to useful methods for analyzing the failure of beams and frames under static loads (1, 5). A criterion has been offered (2, 6) for the estimation of the validity of the same concept in dynamic problems, where the neglect of elastic vibrations is involved. This criterion is based on the hypothesis that a plastic-rigid type of analysis will give good results (as far as the neglect of elastic strains is concerned) when the work done in the plastic deformation greatly exceeds the maximum elastic strain energy that can be stored in the beam. This can be expressed as a requirement that the load (expressed nondimensionally) should sufficiently exceed a certain number which is a constant times the square of the ratio of the duration time of the load to the fundamental period of the beam. However, for this present analysis, we will accept the assumptions of the plastic-rigid theory and not discuss their validity further.

A device frequently employed in studies of dynamic loads on structures is the representation of these structures by semirigid models which consist of a finite number of rigid masses interconnected by springs with proper characteristics. The simplest case is of course the one-dimensional model (Fig. 3) which might be taken as a working approximation of the portal frame of Fig. 2. This approximation might be expected to be valid for certain of the extreme cases, such as where the attached mass is very small, or where it is very large in comparison to the remaining mass. However, in the intermediate cases, it is not obvious how the masses should be lumped in order to obtain reasonably correct results, if indeed reasonable approximations are feasible. One purpose of this report is to give information concerning the accuracy to be expected from solutions obtained by using such a one degree of freedom model.

FORMULATION OF GENERAL DYNAMIC EQUATIONS

We consider the effect of a uniformly distributed load $W(t)$ on a simply supported beam of constant limit moment M_0, constant mass m per unit length, and carrying a concentrated mass Q at its center (Fig. 1). Since it is found that only slight changes occur in the formulae in treating the case of a built-in beam, only the case of simple supports will be discussed in detail, the results for the other case being quoted at the end.

In formulating the kinematical behavior of the beam under the action of the load, we recall that in the plastic-rigid analysis no deformation takes place until the load is such that plastic action can be sustained. We have, therefore, an initial period during which the load builds up (if the load is assumed to start from zero or some small finite value) and the beam is assumed to remain rigid. The problem at this stage is statical, and we readily solve for the maximum moment in the beam, which in this case occurs at the center and attains the value M_0 when $W = 4M_0/l$. The first phase of motion to occur, then, as suggested by the statical moment distribution, would seem to have a plastic hinge at the center (or two hinges infinitesimally close together on either side of the mass). Upon postulating such a condition, however, it is noted that for subsequent deformation to take place, a shear force would be required at the concentrated mass in order to bring it into motion. Such a force cannot be allowed, for, as shown in Fig. 4, it would demand the occurrence of a moment greater than M_0 at some point within the beam. It is therefore concluded that if a hinge appears at the center, it must immediately travel outwards, and for this reason, we consider the first phase of motion to be characterized by two moving hinges as shown in Fig. 5.

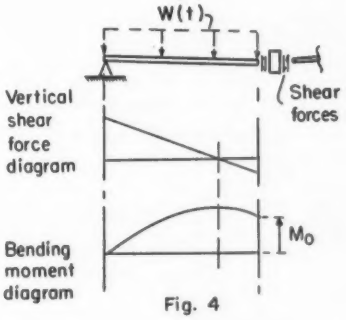

Fig. 4

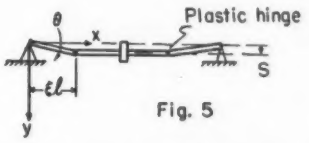

Fig. 5

FIG. 4. Formulation of first phase.
FIG. 5. Deformation mechanism for first phase.

The resulting motion can then be described by the following dynamical equations:
linear impulse-momentum,

$$[1] \qquad \int_{t_0}^{t} W dt - 2\int_{t_0}^{t} R dt = 2\int_{0}^{\xi l} m\left(\frac{dy}{dt}\right) dx + \{2ml[1-\xi]+Q\}\frac{ds}{dt};$$

vertical acceleration of outer portion of beam,

$$[2] \qquad W\xi - 2R = m\xi^2 l^2 \frac{d^2\theta}{dt^2};$$

angular acceleration of outer portion of beam,

$$[3] \qquad \frac{W\xi^2 l}{4} - M_0 = \frac{m\xi^3 l^3}{3}\frac{d^2\theta}{dt^2};$$

vertical acceleration of center portion of beam,

$$[4] \qquad W(1-\xi) = \{2ml[1-\xi]+Q\}\frac{d^2 s}{dt^2};$$

where (see Fig. 5)

x, y — cartesian coordinates,
θ — rotation of outer beam segment,
ξ — dimensionless parameter,
l — beam semispan,
s — transverse displacement of attached mass,
R — reaction at supports,
t_0 — time of start of beam deformation.

Now defining $\mu = Wl/M_0$, $K = Q/2ml$, $\eta = t/\tau$, where τ is a characteristic time of the force pulse, and letting the dot signify differentiation with respect to η, we can reduce the above equations to

$$[5] \qquad \int_{\eta_0}^{\eta}\left\{\mu[1-\tfrac{1}{4}\xi]-\frac{3}{\xi}\right\} d\eta = \dot{s}\frac{ml^2}{m_0\tau^3}\{2-\xi+2K\},$$

$$[6] \qquad \ddot{s}\frac{ml^2}{m_0\tau^3}(1-\xi+K) = \frac{\mu}{2}(1-\xi).$$

In evaluating the integral on the right-hand side of equation [1], we have used the following condition of continuity of transverse velocity:

$$\frac{d\theta}{dt}\xi l = \frac{ds}{dt}.$$

Finally, a single equation is obtained by differentiating equation [5] and solving with equation [6]

$$[7] \qquad (2-\xi+2K)\left\{\mu[1-\tfrac{1}{4}\xi]-\frac{3}{\xi}\right\}+\dot{\xi}\int_{\eta_0}^{\eta}\left\{\mu[1-\tfrac{1}{4}\xi]-\frac{3}{\xi}\right\} d\eta = (2-\xi+2K)^2\frac{\mu(1-\xi)}{2(1-\xi+K)}.$$

A different form of this equation can be obtained by using the jump in transverse acceleration across the traveling hinges as developed in (5). In this case we obtain

$$\ddot{s} = \ddot{\theta}\xi l + \dot{\theta}\dot{\xi} l$$

where $\ddot{s}$ and $\ddot{\theta}$ are given by equations [3] and [4]. The resulting equation, after elimination of $\dot{\theta}$ by differentiation, is

$$[8] \quad \left\{\frac{\mu(1-\xi)}{2(1-\xi+K)} - \frac{3}{4\xi^2}(\mu\xi^2-4)\right\}\ddot{\xi} + \left\{\frac{\mu K}{2(1-\xi+K)^2} + \frac{3}{4\xi^3}(\mu\xi^2+4)\right\}(\dot{\xi})^2 + \left\{\frac{1-\xi+3K}{4(1-\xi+K)}\right\}\mu\dot{\xi} = 0.$$

It appears that, in general, some iterative numerical procedure would have to be used in order to solve either of these equations. However, in considering forms of the pulse $\mu(t)$, we note that previous work on similar problems (3, 4) has shown the total deformation to be largely insensitive to the type of pulse, and hence the selection of a rectangular pulse, which offers considerable analytic simplification, would seem to be a reasonable practical choice. In this case we have

$$\dot{\mu} = \dot{\xi} = 0 \text{ during the pulse } (0 \leqslant t \leqslant \tau),$$

$$\mu = 0 \text{ after the pulse } (\tau < t).$$

Equation [7] can then be rewritten

$$[9] \quad \mu_0 = \frac{12(1-\xi_0+K)}{\xi_0^2(1-\xi_0+3K)}.$$

Equation [9] can be used to determine the initial position of the hinges for pulses starting with a finite value $\mu \geqslant 4$, as well as giving the position of the hinges during the action of a rectangular pulse. Fig. 6 shows a plot of this equation for the full range of the parameter K.

For K approaching zero, which represents the case treated in (4), we note that the hinges remain at the center of the beam for values of the load $4 \leqslant \mu \leqslant 12$ and spread into finite plastic regions for higher loads, in accordance with the results obtained therein. We also note, in the present problem, the appearance of a new phase for higher loads, where a negative plastic moment is developed at the center because of the inertial resistance of the concentrated mass. The criterion for the appearance of this next phase can be obtained by solving for the moment at the center of the inner beam section, which is illustrated in Fig. 7. Setting the moment at the center equal to $-M_0$, we obtain

$$[10] \quad \xi = 1 - \frac{1+\sqrt{1+\frac{1}{4}\mu K^2}}{\frac{1}{4}\mu K}.$$

The intersection of the curves defined by equation [9] with those of equation [10] is shown by the broken line in Fig. 6, which thus defines the upper boundary of the first phase.

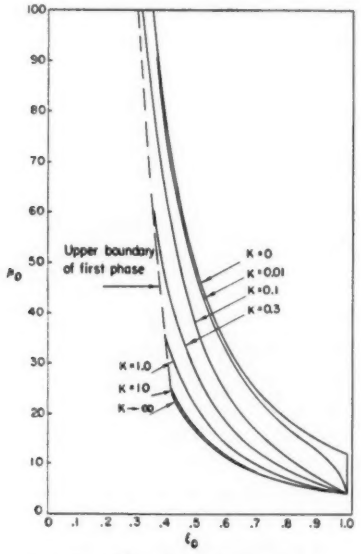

FIG. 6. First phase hinge locations.

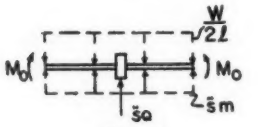

Fig. 7

Fig. 8

FIG. 7. Inner beam segment as a free body.
FIG. 8. Deformation mechanism for second phase.

The mechanism of the second phase is shown in Fig. 8. Using the same procedure as before, we obtain the following equations of motion:
linear impulse-momentum,

$$[11] \qquad \int_{\eta_0}^{\eta} \left\{ \mu[1-\tfrac{1}{2}\xi] - \frac{3}{\xi} \right\} d\eta = \frac{ml^3}{M_0\tau^2}\,\theta\xi[2-\xi] + \dot{\alpha}[1-2\xi+\xi^2] + \frac{2K\dot{s}}{l};$$

continuity of transverse velocity,

$$[12] \qquad \dot{s} = \dot{\theta}\xi l + \dot{\alpha}(1-\xi)l;$$

jump in transverse acceleration,

$$[13] \qquad \ddot{s} = \ddot{\theta}\xi l + \dot{\xi}l(\dot{\theta}-\dot{\alpha}) + \ddot{\alpha}(1-\xi)l;$$

acceleration of concentrated mass,

[14] $$\ddot{s}\frac{ml^2}{M_0\tau^2} = \frac{24+\mu(1-\xi)^2}{2(1-\xi)(1-\xi+4K)};$$

angular acceleration of inner beam segment,

[15] $$\ddot{\alpha}\frac{ml^3}{M_0\tau^2} = \frac{24(1-\xi+K)-3\mu K(1-\xi)^2}{(1-\xi)^3(1-\xi+4K)};$$

and angular acceleration of outer beam section,

[16] $$\ddot{\theta}\frac{ml^3}{M_0\tau^2} = \frac{3}{4\xi^3}(\mu\xi^2-4).$$

We can now formulate the general equation of motion by using either equation [11] or [13] as a basis, and employing equations [12], [14], [15], and [16] as required. Either of these formulations, however, results in an unwieldy non-linear equation which does not appear to lend itself to analytical treatment. For the special case of the rectangular load pulse, we can use equations [13], [14], [15], and [16] to obtain

[17] $$\mu_0 = \frac{(12/\xi_0^2)(1-\xi_0)^2(1-\xi_0+4K)-48(1-\xi_0+2K)}{(1-\xi_0)^3}.$$

A plot of the curves defined by equation [17] is shown in Fig. 9. It is noted that during this phase ξ_0 becomes independent of M_0 for infinite K, which corresponds to the case of a uniform beam simply supported at one end and built in at the other.

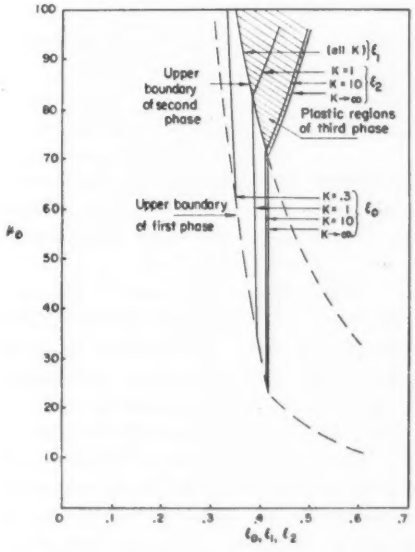

FIG. 9. Second and third phase "hinge" locations.

A third phase can be identified by noting the conditions under which the plasticity condition is violated in the second phase, i.e., when a moment greater than M_0 is developed at some point in the beam. If we consider the outer beam segment first, we see that the plasticity condition might be violated only at the hinge end, since the moment must be zero at the simple support and increase on going inward. The condition that the moment decreases steadily from M_0 on going outward from the hinge is obtained from the requirement that d^2M/dz^2 is of one sign in this segment. The following condition ensures this:

$$m\ddot{\xi}\ddot{\theta} \leqslant W\tau^2/2l\,. \tag{18}$$

The critical value is found by using the equality sign in equation [18], and this with equation [16] reduces to

$$\mu\xi_1^2 = 12, \tag{19}$$

where the subscript is now used to denote the particular plastic-rigid interface.

In the case of the inner beam segment, we have a moment distribution as shown in Fig. 10. From the shape of this moment curve it is clear that no violation of the plasticity condition can occur near the inner end of this segment. Such a violation would, however, occur at the outer (traveling hinge) end of the segment if d^2M/dz^2 changed sign near this end. The condition that no violation occurs is

$$ma_0 \leqslant W\tau^2/2l, \tag{20}$$

a_0 being the acceleration of the outer tip of this section. Now we have

$$a_0 = \ddot{s} - \ddot{\alpha}(1 - \xi)l. \tag{21}$$

Using equation [20] with an equality sign, together with equations [14], [15], and [21], we obtain the criterion

$$\mu = \frac{24(1-\xi_2+K)-12(1-\xi_2)}{K(1-\xi_2)^2}\,. \tag{22}$$

A plot of the curves defined by equation [22] has been included in Fig. 9, where their intersection at the same point with the curve defined by equation [19] and the appropriate curves of equation [17] furnishes a check of our assumed deformation mechanism.

The third, and now necessarily final phase, thus has two finite plastic zones as shown in Fig. 11. An initially infinite load thus would imply that the entire beam is instantaneously plastic. The boundaries of the plastic zone are defined by equations [19] and [22] for the case of the rectangular pulse during the time of its action or for an increasing load. After such a pulse, or for a decreasing pulse, equations [19] and [22] become only inequalities and either impulse-momentum equations, such as equation [11], or an acceleration jump equation, such as equation [13], are required to describe the motion. However, we shall not carry through the analytical treatment for this phase, and will limit ourselves to maximum values of μ_0 below about 70 so that only the first and second phases occur.

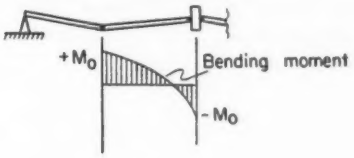

Fig. 10

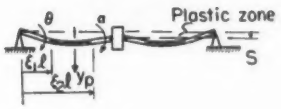

Fig. 11

Fig. 12

FIG. 10. Moment distribution for inner beam segment.
FIG. 11. Deformation mechanism for third phase.
FIG. 12. Deformation mechanism for final motion.

BEAM DEFORMATION

The deformation of the beam is best described by the transverse displacement of the concentrated mass and the angular displacements at the ends and at the center. Considering the transverse displacement first, the complete displacement consists of the following parts:

(1) Displacement s_1 during the time of action $(\eta_1 - \eta_0)$ of the load pulse.

(2) Displacement s_2 during the interval $(\eta_2 - \eta_1)$ when the motion corresponds to the kinematical picture of Fig. 11. This interval ends when the finite plastic zones are reduced to point hinges.

(3) Displacement s_3 during the interval $(\eta_3 - \eta_2)$ when the motion corresponds to the kinematical picture of Fig. 8. This interval ends when the angular velocities of the inner segments vanish.

(4) Displacement s_4 during the interval $(\eta_4 - \eta_3)$ when the motion corresponds to the kinematical picture of Fig. 5. This interval ends when the traveling outer hinges reach the center of the beam.

(5) Displacement s_5 during the interval $(\eta_5 - \eta_4)$ when the motion corresponds to the kinematical picture of Fig. 12. This interval ends when the angular velocities of the half-beams vanish.

For the general case of a load starting from zero and gradually increasing, the displacement s_1 is subdivided into three displacements occurring during the three phases of motion. In the case of loads initiating only the first and second phases, s_2 is zero, and when only the first phase is initiated, s_2 and s_3 are zero.

For rectangular load impulses (which we are considering) the displacement

s_1 is obtained by direct integration of equation [6] for the first phase, and of equation [14] for the second phase. The resulting expressions are:
load producing first phase

$$s_1 \frac{ml^3}{M_0\tau^2} = \frac{\mu_0(1-\xi_0)}{4(1-\xi_0+K)},$$

load producing second phase

$$s_1 \frac{ml^2}{M_0\tau^2} = \frac{24+\mu_0(1-\xi_0)}{4(1-\xi_0)(1-\xi_0+4K)}.$$

Assuming the load magnitude to be such that $s_2 = 0$, we have next to find the displacement s_3 by solving either equation [11] or [13] with $\mu = 0$ and ξ being variable. Because of the non-linearity of these equations a numerical integration would be required to obtain exact results. However, an approximate solution can be obtained by recalling that during the second phase ξ remained essentially constant for the smaller values of load. We therefore inquire into the value of $\dot{\xi}$ during the second interval $\eta_3 - \eta_1$ to see if a similar behavior occurs. We will restrict ourselves to values of μ_0 not greater than 50, and as a first approximation, will calculate the value of $\dot{\xi}$ at the beginning and end of the interval for the same value of ξ.

Using equations [13], [14], [15], and [16] we obtain

[23] $$\dot{\xi} \frac{ml^3}{M_0\tau^2} = \frac{12\xi^2(1-\xi+2K)-3(1-\xi)^2(1-\xi+4K)}{\xi^2(1-\xi)^2(1-\xi+4K)(\dot{\theta}-\dot{\alpha})}$$

where at the beginning of the motion

$$(\dot{\theta}-\dot{\alpha}) \frac{ml^3}{M_0\tau^2} = \frac{3}{4\xi_0^3}(\mu_0\xi_0^2 - 4) - \frac{24(1-\xi_0+K)-3\mu_0K(1-\xi_0)^2}{(1-\xi_0)^3(1-\xi_0+4K)}.$$

The approximate value of the angular velocity difference at the end of the motion is

$$(\dot{\theta}-\dot{\alpha}) \frac{ml^3}{M_0\tau^2} = \frac{3\mu_0}{4\xi_0^3}\left\{\xi_0^2 - \frac{K(1-\xi_0)^2}{2(1-\xi_0+K)}\right\}$$

where we have used the value

[24] $$\eta_3 = \frac{\mu_0K(1-\xi_0)^2}{8(1-\xi_0+K)}$$

which is obtained by setting $\dot{\alpha} = 0$.

For large K, the numerator in equation [23] tends to zero while the denominator remains finite; thus for $K = 10$, $\mu_0 = 50$, the approximate initial value of $\dot{\xi}$ is 0.003. For $K = 1$, $\mu_0 = 50$, the approximate initial and final values of $\dot{\xi}$ are 0.03 and 0.07, with the approximate value of $(\eta_3 - \eta_2) = (\eta_3 - \eta_1)$ being 0.4. Only a small variation in ξ is therefore indicated, and comparison with results obtained by an iterative numerical procedure using equations [11], [14], [15], and [16] shows that for this range of μ_0, the assumption of constant ξ during the second interval gives final deformation values within three per cent of the exact values.

Using this approximation of constant ξ, we readily obtain the following relations:

[25] $$\dot{s}_3 \frac{ml^2}{M_0\tau^2} = \frac{24\eta_3+\mu_0(1-\xi_0)^2}{2(1-\xi_0)(1-\xi_0+4K)},$$

[26] $$s_3 \frac{ml^2}{M_0\tau^2} = \frac{12(\eta_3^2-1)+\mu_0(1-\xi_0)^2(\eta_3-1)}{2(1-\xi_0)(1-\xi_0+4K)},$$

where η_3 is defined by equation [24]. The velocity $\dot{s}_3$, of the concentrated mass at the end of the second motion, has been included because of its usefulness in computing the remaining displacements.

For the motion in the next interval, $(\eta_4 - \eta_3)$, we set $\mu = 0$ in equation [5] to obtain

[27] $$\int_0^1 \left\{\mu_0[1-\tfrac{1}{3}\xi_0]-\frac{3}{\xi_0}\right\} d\eta - \int_1^\eta \frac{3}{\xi}\, d\eta = \dot{s}\,\frac{ml^2}{M_0\tau^2}\,(2-\xi+2K).$$

We proceed by differentiating equation [27], noting that equation [4] shows $\dot{s}$ to be constant during this type of motion. Subsequent integration then yields

$$\frac{\xi^2}{2}\frac{ml^2}{M_0\tau^2} = \frac{3}{\dot{s}_3}+c$$

where c is evaluated at $\eta = 1$, $\xi = \xi_0$. The time η_4, determined by setting $\xi = 1$, is then

$$\eta_4 = \eta_3+\dot{s}_3\frac{ml^2}{M_0\tau^2}\left(\frac{1-\xi_0^2}{6}\right).$$

The corresponding displacement can then be written as follows:

$$s_4\frac{ml^2}{M_0\tau^2} = \left\{\dot{s}_3\frac{ml^2}{M_0\tau^2}\right\}^2\left\{\frac{1-\xi_0^2}{6}\right\}.$$

The mechanism of the final motion is illustrated in Fig. 12. Moment equilibrium of the half-beam gives

[28] $$\ddot{s}\frac{ml^2}{M_0\tau^2} = \frac{-3}{(1+3K)}.$$

Integrating once and evaluating the constant at $\eta = \eta_4$, $\dot{s} = \dot{s}_3$, we obtain

$$\eta-\eta_4 = (\dot{s}_3-\dot{s})\frac{ml^2}{M_0\tau^2}\left(\frac{1+3K}{3}\right).$$

The motion ceases when $\dot{s} = 0$, or

$$\eta_5-\eta_4 = \dot{s}_3\frac{ml^2}{M_0\tau^2}\left(\frac{1+3K}{3}\right).$$

Performing a further integration, and using the conditions that when $\eta = \eta_4$, $s = 0$ and when $\eta = \eta_5$, $s = s_5$, we get

$$s_5\frac{ml^2}{M_0\tau^2} = \left\{\dot{s}_3\frac{ml^2}{M_0\tau^2}\right\}^2\left\{\frac{1+3K}{6}\right\}$$

which can be reduced to

$$s_5 \frac{ml^2}{M_0\tau^2} = \left\{\frac{\mu_0(1-\xi_0)}{(1-\xi_0+K)}\right\}^2\left\{\frac{1+3K}{24}\right\}.$$

The total transverse displacement can then be written

$$[29] \quad s\frac{ml^2}{M_0\tau^2} = \frac{24\eta_3{}^2+\mu_0(1-\xi_0)^2(2\eta_3-1)}{4(1-\xi_0)(1-\xi_0+4K)}+\left\{\dot{s}_3\frac{ml^2}{M_0\tau^2}\right\}^2\left\{\frac{2-\xi_0^2+3K}{6}\right\}$$

where η_3 and $\dot{s}_3$ are given by equations [24] and [25]. For the case of load pulses initiating only the first phase, the expression reduces to

$$[30] \quad s\frac{ml^2}{M_0\tau^2} = \frac{\mu_0(1-\xi_0)}{2(1-\xi_0+K)}\left\{\frac{1}{2}+\frac{\mu_0(1-\xi_0)}{2(1-\xi_0+K)}\left[\frac{2-\xi_0{}^2+3K}{6}\right]\right\}.$$

A plot of equations [29] and [30] is shown in Fig. 13. In the special case where $K = 0$ and $\xi_0 = 1$ simultaneously, equation [30] can be evaluated only by using a limiting process. A simpler procedure is to note that the proper expression to be used for the velocity $\dot{s}$ is easily obtained from equation [16] by putting $\xi = \xi_0 = \text{constant}$; the result is

$$\dot{s}\frac{ml^2}{M_0\tau^2} = \frac{3}{4\xi_0{}^2}(\mu_0\xi_0{}^2-4).$$

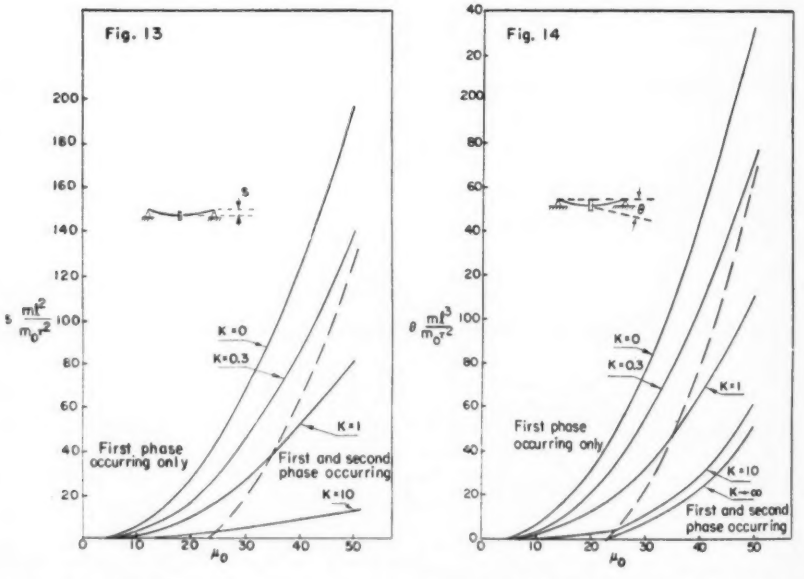

FIG. 13. Displacement at center due to a uniformly distributed rectangular load pulse (simply supported beam).

FIG. 14. Angular displacement at end due to a uniformly distributed rectangular load pulse (simply supported beam).

Using this expression with $\xi_0 = 1$, equation [30] becomes

$$[31] \qquad s\frac{ml^2}{M_0\tau^2} = \frac{3}{32}\mu_0(\mu_0-4),$$

as obtained in (4) for the condition of $K = 0$ and $4 \leqslant \mu_0 \leqslant 12$.

The angular displacement at the ends of the beam is determined in a manner completely analogous to that of the transverse displacement, the result being

$$[32] \quad \theta\frac{ml^3}{M_0\tau^2} = \frac{3}{8\xi_0^3}\left\{\mu_0\xi_0^2[2\eta_3-1]-4\eta_3^2\right\}+\left\{s_3\frac{ml^2}{M_0\tau^2}\right\}^2\left\{\frac{1-2\xi_0+3K}{6}\right\}.$$

When the second phase does not occur the expression is:

$$[33] \quad \theta\frac{ml^3}{M_0\tau^2} = \frac{3}{8\xi_0^3}(\mu_0\xi_0^2-4)+\left\{\frac{\mu_0(1-\xi_0)}{2(1-\xi_0+K)}\right\}^2\left\{\frac{1-2\xi_0+3K}{6}\right\}.$$

A plot of equations [32] and [33] is given in Fig. 14.

For the case of K approaching infinity, the behavior tends to resemble that of two separate uniform beams, and thus gives an insight into the formation of the plastic-rigid deformation mechanism for a uniform beam built-in at one end and simply supported at the other, when the built-in support is allowed to be displaced. For infinite K, the resemblance to the case of two uniform beams is exact, and no deformation occurs until the load reaches the critical value which initiates the second phase. This value of the load is easily found to be $\mu_0 = 23.315$ with the corresponding value of ξ_0 being 0.4142.

In addition to the transverse displacement at the center and the angular displacement at the ends, an important measure of damage for certain ranges of μ_0 and K may be the angular displacement at the concentrated mass. It is interesting to note that when the load is high enough to produce the second phase, yielding occurs under negative moment (0 to η_3) followed by yielding under positive moment (η_4 to η_5). This reversal of the plastic flow in a problem of dynamic loading of a structure appears to have been observed here for the first time. It may have important significance in connection with the possibility of rupture of the beam.

The angular displacement at the concentrated mass is described by the following expressions:

(*a*) for loads producing the first phase

$$\alpha_1 = \alpha_2 = \alpha_3 = \alpha_4 = 0,$$

$$\alpha_5\frac{ml^3}{M_0\tau^2} = \left\{\frac{(1-\xi_0)}{(1-\xi_0+K)}\right\}^2\left\{\frac{1+3K}{24}\right\},$$

and the time variation is given by

$$\alpha\frac{ml^3}{M_0\tau^2} = \frac{(1-\xi_0)}{2(1-\xi_0+K)}(\eta-\eta_4)-\frac{3}{2(1+3K)}(\eta-\eta_4)^2;$$

(*b*) for loads producing the second phase,

$$\alpha_1 \frac{ml^3}{M_0\tau^2} = \frac{24(1-\xi_0+K)-3\mu_0K(1-\xi_0)^2}{2(1-\xi_0)^3(1-\xi_0+K)},$$

$$\alpha_2 = 0,$$

$$\alpha_3 \frac{ml^3}{M_0\tau^2} = \frac{-3\{\mu_0K(1-\xi_0)^2-8(1-\xi_0+K)\}^2}{16(1-\xi_0)^3(1-\xi_0+4K)(1-\xi_0+K)},$$

$$\alpha_4 = 0,$$

$$\alpha_5 \frac{ml^3}{M_0\tau^2} = \left\{\frac{\mu_0(1-\xi_0)}{(1-\xi_0+K)}\right\}^2\left\{\frac{1+3K}{24}\right\}.$$

A plot of the above results is shown for two cases in Fig. 15. In the first case, the load is just under that for the second phase, while in the second case, the second phase is excited and the reversal of plastic flow is displayed.

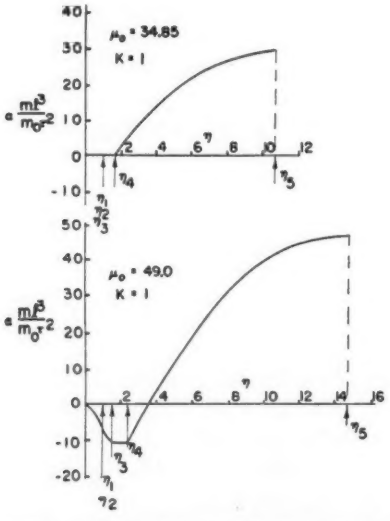

FIG. 15. Time variation of angular displacement at the mass.

The deformation mechanism for the first phase in the case of a built-in beam is shown in Fig. 16. The only changes which occur in the dynamical equations are the values of certain constants. For this reason, all intermediate steps in their development are omitted, and only the final equations are shown below.

[5*A*] $$\int_{\eta_0}^{\eta}\left\{\mu[1-\tfrac{1}{4}\xi]-\frac{6}{\xi}\right\}d\eta = \tfrac{1}{3}\frac{ml^2}{M_0\tau^2}(2-\xi+2K),$$

[9*A*] $$\mu_0 = \frac{24(1-\xi_0+K)}{\xi_0^2(1-\xi_0+3K)},$$

$$[11A] \quad \int_{\eta_0}^{\eta}\left\{\mu[1-\tfrac{1}{4}\xi]-\frac{6}{\xi}\right\}d\eta = \frac{ml^3}{M_0\tau^2}\left\{\theta\xi[2-\xi]+\dot{\alpha}[1-2\xi+\xi^2]+\frac{2K\dot{s}}{l}\right\},$$

$$[17A] \quad \mu = \frac{(24/\xi_0^2)(1-\xi_0)^2(1-\xi_0+4K)-48(1-\xi_0+2K)}{(1-\xi_0)^3},$$

$$[28A] \quad \ddot{s}\frac{ml^3}{M_0\tau^2} = \frac{6}{1+3K}.$$

The corresponding expressions for the total deformations are

$$[29A] \quad s\frac{ml^2}{M_0\tau^2} = \frac{24\eta_3^2+\mu_0(1-\xi_0)^2(2\eta_3-1)}{4(1-\xi_0)(1-\xi_0+4K)}+\left\{\dot{s}_3\frac{ml^2}{M_0\tau^2}\right\}^2\left\{\frac{2-\xi_0^2+3K}{12}\right\},$$

$$[30A] \quad s\frac{ml^2}{M_0\tau^2} = \frac{\mu_0(1-\xi_0)}{2(1-\xi_0+K)}\left\{\frac{1}{2}+\frac{\mu_0(1-\xi_0)}{2(1-\xi_0+K)}\left[\frac{2-\xi_0^2+3K}{12}\right]\right\},$$

$$[32A] \quad \theta\frac{ml^3}{M_0\tau^2} = \frac{3}{8\xi^3}\{\mu_0\xi_0^2[2\eta_3-1]-8\eta_3^2\}+\left\{\dot{s}_3\frac{ml^2}{M_0\tau^2}\right\}^2\left\{\frac{3-2\xi_0+3K}{12}\right\},$$

$$[33A] \quad \theta\frac{ml^3}{M_0\tau^2} = \frac{3}{8\xi^3}(\mu_0\xi_0^2-8)+\left\{\frac{\mu_0(1-\xi_0)}{2(1-\xi_0+K)}\right\}^2\left\{\frac{3-2\xi_0+3K}{12}\right\}.$$

The values of η_3 and $\dot{s}_3$ are given by equations [24] and [25] respectively. A plot of equations [32A] and [33A] is shown in Fig. 18.

Fig. 16

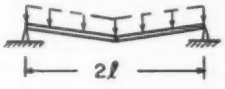

Fig. 17

FIG. 16. Deformation mechanism for the first phase of the built-in beam.
FIG. 17. Deformation mechanism for the first phase of the uniform beam.

USE OF A SIMPLE MODEL

A standard technique employed in engineering analysis of structures under dynamic loading is the replacement of the structure by a model having a finite number of degrees of freedom. The simplest such model is the single mass-spring system (Fig. 3) of one degree of freedom. As noted in (4), if in our problem we assume the beam to be displaced in a definite deflection curve, we reduce its infinite number of degrees of freedom to only one, thus making a single degree of freedom model the appropriate simple counterpart. Under these conditions, the properties of the model can be chosen so that the displacement of the model corresponds exactly to the deflection of, for example, the midpoint of the beam. However, if (as in the beam problem considered here) the deflection curve changes its shape during the course of the motion, the one-dimensional model can give exact results only during that part of the motion in which the selected mode is maintained.

One procedure for reducing the real structure to the simple model, once the form of the model has been decided upon, is to relate the applied loads, which

in our case are the distributed load for the beam problem and the concentrated load for the model, so that the work done is the same in each case; and to choose a mass for the model so that its total kinetic energy is the same as that of the beam moving in the assumed deflection curve.

In the case of a simply supported uniform beam, for values of the load in the range $4 \leqslant \mu_0 \leqslant 12$, a plastic hinge occurs only at the center of the beam (Fig. 17). There is therefore only one mode, and we obtain exact results by using a simple model. Following the procedure outlined above, we equate the

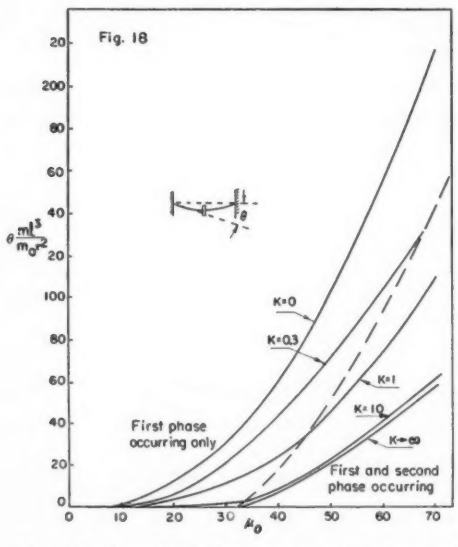

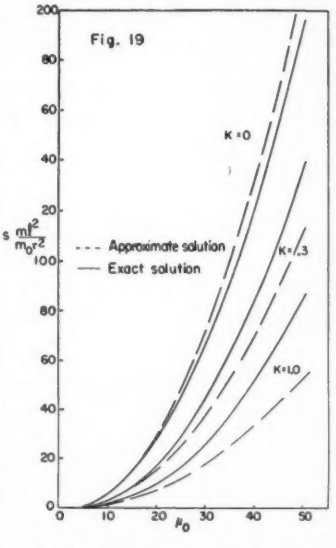

FIG. 18. Angular displacement at end due to a uniformly distributed rectangular load pulse (built-in beam).
FIG. 19. Comparison of approximate and exact solutions for the displacement at the center due to a rectangular load pulse (simply supported beam).

work done by P and W to obtain $P = W/2$, and similarly equating the kinetic energies we find $M = \frac{2}{3}ml$. Lastly, we equate the works done by the resistive forces to obtain $F = 2M_0/l$. Now for the simple model, where we allow the spring to offer plastic resistance only, the expression for the total displacement resulting from a rectangular load impulse of magnitude P and duration τ is

$$[34] \qquad s\frac{M}{F\tau^2} = \frac{P}{2F}\left\{\frac{P}{F}-1\right\}.$$

Substituting the relationships determined for P, M, and F into this equation, we obtain

$$[35] \qquad s\frac{ml^2}{M_0\tau^2} = \frac{3}{32}\mu_0(\mu_0-1)$$

which is identical with the exact expression (equation [31]) as furnished by a direct solution of the beam problem for μ_0 in the stated range.

From the complete solution of the beam problem (4), we know that for $\mu_0 > 12$, the appearance of a finite plastic zone introduces a new kinematical behavior, which is reflected in the expression for the deformation. However, had we proceeded only with the model, we would have had no means of accounting for this phase, and Fig. 19 has been included to show the error incurred by using the elementary expression beyond its range of validity.

Considering now the problem of a beam carrying a concentrated mass, one might expect that the replacement of the actual system by a one-dimensional model would be more satisfactory than in the case of the uniform beam. The natural beam configuration to assume in the reduction to the one-dimensional system is again the configuration of Fig. 17, except that the central "hinge" now consists of two hinges adjacent to mass Q, as in Fig. 12. Using the same procedure as before in obtaining the correspondence between variables, the only change found to occur is in the expression for the mass M of the model, which now becomes

$$M = \tfrac{2}{3}ml + Q.$$

Substitution into equation [33] yields the result

$$s\frac{ml^2}{M_0\tau^2} = \frac{3\mu_0}{32(1+3K)}(\mu_0-4).$$

A comparison of this result with the exact results for two values of K is also shown in Fig. 19. The error is noted to be relatively small and positive for $K \approx 0.2$, and, contrary to expectation, to become increasingly large and negative for large values of K.

In an attempt to improve the approximate results, a second choice for the configuration might be that shown in Fig. 5. With this configuration, the equivalence procedure with the one-dimensional model leads to the following relations:

$$P = W\{\tfrac{1}{2}(2-\xi_0)\},$$
$$M = ml\{\tfrac{1}{3}(6-4\xi_0)\} + Q,$$
$$F = 2M_0/\xi_0 l.$$

Using equation [34], the new expression for the total deformation is

$$s\frac{ml^2}{M_0\tau^2} = \frac{3(2-\xi_0)\,\mu_0}{32(3-2\xi_0+3K)}(\mu_0[2-\xi_0]\,\xi_0-4).$$

However, a numerical analysis shows that, although some improvement can be effected by choosing ξ_0 to be approximately 0.9, it is negligible in comparison to the total error.

We have already noted that as K becomes large, the behavior during the deformation tends to resemble that of two uniform beams built in at the center. This might suggest the alternative approach of actually treating the problem as two uniform beams for the case of large K. However, since the deformation obtained by these results would not commence until μ_0 attained a value of 23.315 for the simply supported beam, and 32.0 for the built-in beam, it could

hardly be accurate for values of μ_0 of this order for K ranging from say 1 to 5, for at these values of μ_0 and K, Figs. 13, 14, and 18 already show appreciable deformation. We note, of course, that for both large μ_0 and K, the most important parameter is the angular deflection at the ends. However, the model we have used is not directly amenable to duplicate angular displacement, and the simple expedient of dividing its answers by l leads to grossly inaccurate results for large K. We might, alternatively, consider a different model which incorporates angular instead of rectilinear motion, but it is evident that for values of K ranging from 1 to 5, and μ_0 of the order 30, the generally radical changes experienced by the deflection curve could not be effectively duplicated by any simple one-dimensional model. A better account might be made of the original continuum problem if further characteristics were added to the model, but this would seem to defeat the essential purpose of simplicity for which the model was introduced.

CONCLUSIONS

A simply supported or built-in beam, carrying a concentrated mass at its center, may experience as many as seven distinct patterns of deformation during its whole deformation process resulting from a uniformly distributed load pulse. The first effect of a small but finite mass at the center is to prevent the development of a centered plastic zone which appears in the second deformation phase of a uniform beam. As the relative size of this mass is increased, a new second phase becomes important. This second phase is characterized by an additional plastic hinge at the center where the direction of deformation, as shown in Fig. 8, is opposite to that which occurs in the uniform beam case. When the ratio of the attached mass to the beam mass becomes of the order of ten or greater, the deformation behavior closely resembles that of two uniform beams, with their inner supports being built-in.

A second effect of the attached mass is the occurrence of a reversal in the plastic flow at the middle of the beam when the load is high enough to initiate the second phase. This behavior may have an important influence on the tendency of the beam to fracture and hence the present results may provide a useful parameter in formulating an experimental criterion for beam failure.

The technique of approximating a continuous structure by a simple model in dynamical problems provides good results only when the motions to be accounted for are nearly identical, so that they may be closely described by using only a small number of parameters as provided by the simple model. In the case of a uniform beam acted upon by a small transverse load, only one deformation mode occurs, and hence a one-dimensional model can be constructed to duplicate exactly any chosen characteristic of the deformation. However, if a concentrated mass is attached to the beam, or if high values of load are employed, marked changes may occur in the mode of deformation and a simple one-dimensional model in general gives erroneous results, though fair approximations may possibly be obtained for restricted ranges of the parameters involved.

ACKNOWLEDGMENT

The author wishes to express his thanks to Professor P. S. Symonds for his suggestion of this problem and for his helpful advice.

REFERENCES

1. Baker, J. F. J. Inst. Civil Engrs. (London), 31: 188–224. 1949.
2. Lee, E. H. and Symonds, P. S. Trans. ASME, 19: 308–314. 1952.
3. Symonds, P. S. Trans. ASME, 20: 475–481. 1953.
4. Symonds, P. S. Large plastic deformations of beams under blast type loading. Tech. Rept. No. 99. Contract N7onr-35801 with the Office of Naval Research.
5. Symonds, P. S. and Neal, B. G. J. Franklin Inst. 252: 383–407. 1951.
6. Symonds, P. S. and Leth, C-F. A. Impact of finite beams of ductile metal. Tech. Rept. No. 20. Contract N7onr-35810 with the Office of Naval Research.

SOME CHARACTERISTICS OF SPRAY-DRIED WHEAT GLUTEN[1]

By W. B. McConnell

ABSTRACT

Dispersions of wheat gluten in 0.01 *N* acetic acid were spray dried using various drying conditions to give powders retaining most of the original baking strength of the gluten. The dispersions had a pH near 5.4 and for most experiments they contained from 8 to 9% solids. With the spray drying equipment used an inlet drying air temperature of 160° C. and outlet temperature of 90° C. consistently gave gluten which compared favorably with that obtained by freeze drying. Baking (100-gm. loaves) data obtained after addition of spray-dried gluten to a cake flour gave a regression coefficient for loaf volume on per cent protein added of 48.2. The preparations contained 15.4±0.3% nitrogen and could be readily redispersed in 0.1 *N* acetic acid. The moisture content of the freshly dried gluten preparations ranged from 0.4 to 4%; however they adsorbed atmospheric moisture and at 90% relative humidities they became wet and gummy. The preparations were uniform, consisting largely of spherical powder particles with diameters between 10 and 20 microns. It is concluded that it is technically feasible to prepare and use spray-dried gluten for improving the baking quality of low protein flour.

INTRODUCTION

In 1950 Lusena (3) described a method for preparing a dispersion of pure wheat gluten in dilute acetic acid solutions and showed that the gluten obtained by freeze drying the dispersions was essentially undenatured. Preliminary work by Lusena and Adams (4) indicated that the gluten dispersions could be spray dried to give a finely powdered product retaining much of its bread-making quality. This work has been extended to evaluate the practicability of spray drying gluten for use as a flour additive in the baking industry.

This communication reports on the nature and baking characteristics of spray-dried wheat gluten. It includes some observations on the effects of variations in the drying process on the quality of the product and gives data related to physical characteristics of significance when considering its possible production on a commercial scale.

EXPERIMENTAL

Preparation of Gluten Dispersions

Acetic acid dispersions of gluten from an unimproved top patent flour (12.8% protein) were made according to the method outlined by Lusena (3). A laboratory homogenizer (Eppenback Homomixer No. 2) was used to disperse the gluten in 0.005 *N* acetic acid. Four minutes' agitation at full speed was sufficient for thorough dispersion of the gluten from 1500 gm. flour. The gluten was precipitated with calcium hydroxide, and redispersed for drying in 0.01 *N* acetic acid (3). The second dispersion had a pH near 5.4 and contained from 8 to 9% solids. The nitrogen content of the dry solids was 15.4%.

[1]*Manuscript received February 4, 1955.*
Contribution from the National Research Council of Canada, Prairie Regional Laboratory, Saskatoon, Saskatchewan. Issued as Paper No. 189 on the Uses of Plant Products and as N.R.C. No. 3622. Presented in part at the Annual Conference of the Chemical Institute of Canada at Windsor, Ontario, June 1953.

Spray Drying Method

The gluten dispersions were dried in an insulated stainless steel spray drier with a maximum inner diameter of 24 in. It was constructed according to the detail of Woodcock and Tessier (7).

In operation, the drier was first fed with acetic acid until temperature equilibrium at the desired conditions was attained. After the gluten dispersion was admitted through the spray nozzle minor adjustments were usually necessary to maintain the initial temperature conditions. After drying was completed the feed lines were flushed again with dilute acetic acid.

A number of preliminary experiments were necessary to obtain a satisfactory adjustment of the atomizing nozzle and atomizing air pressure. If the spray was coarse some undried droplets reached the inner surface of the cone where they were deposited as a hard coating, adhering firmly to it. The same difficulty was encountered with a wide-angle spray. Wide sprays also increased deposition of gluten on the spraying nozzle with a resultant distortion of the spray pattern and eventual clogging of the nozzle. Best results were obtained from a fine spray with the droplets directed well toward the apex of the cone. An atomizing air pressure of 25 p.s.i. was used in all reported experiments.

About half of the dried gluten collected as a fine white powder in the receiving jar, and in the bottom of the cone. This was designated as Fraction A. A considerable amount of material adhered loosely to the upper portion of the walls and was collected by brushing and rubbing the lining of the drier (Fraction B).

Comparison of the two fractions was made throughout the whole series of experiments. In general Fraction A was only slightly superior to Fraction B in baking quality, but it was considerably more uniform in particle size and had a greater bulk density. The material which adhered to the walls of the drier came, at least in part, from droplets that reached the sides of the cone before they were completely dry. Since this difficulty would likely not be encountered with a larger spray drier the free powder was considered to be more characteristic of a spray-dried gluten. Results reported herein are therefore limited to those obtained with Fraction A.

Analytical Methods and Baking Tests

Nitrogen determinations were done by the conventional Kjeldahl methods. Moisture contents of the preparations were obtained from the loss in weight of samples heated at 110° C. for 20 hr., and total solids in the dispersions were measured by evaporating aliquots to dryness.

Samples of freeze-dried gluten dispersions were prepared with a laboratory-scale glass lyophil apparatus (6).

The gluten quality was evaluated by observing its ability to improve the bread-making quality of a low protein flour. For the experiments in which the drying conditions were varied, a 9.3% protein pastry flour was raised to 15% protein by addition of the spray-dried preparations. The somewhat larger than normal final protein content was advantageous for detecting differences in gluten quality.

The gluten and the base flour were mixed dry and the resulting flour was test-baked, using a sugar-rich baking formula which maintains adequate gas production throughout the baking procedure* and thus permits the evaluation of flour strength. The volumes of the loaves were measured. The loaves then were scored for external characteristics and photographed to provide a permanent record.

EXPERIMENTAL RESULTS

Effect of Drying Temperatures on Gluten

Table I contains a summary of data obtained to characterize gluten samples prepared by operating the spray drier with a series of different inlet and outlet

TABLE I

BAKING CHARACTERISTICS AND MOISTURE CONTENTS OF GLUTENS SPRAY DRIED WITH DIFFERENT INLET AND OUTLET AIR TEMPERATURES

Exp. No.	Outlet temp., °C.	Inlet temp., °C.	% N in dry solids	Fraction A	
				Moisture, %	Av. loaf volume, cc. (pastry flour base)
1	80	170	15.3	1.85	795
2	80	160	15.5	1.20	750
4	80	140	15.6	1.68	750
5	80	130	15.1	2.70	730
6	90	170	15.5	3.66	835
7	90	160	15.2	1.22	845
8	90	150	15.3	2.23	715
9	90	140	15.7	0.78	735
10	100	170	15.2	1.58	710
11	100	160	15.2	1.14	740
12	100	150	15.6	2.65	775
13	100	140	15.6	0.83	740
14	110	170	15.5	0.40	725
15	110	160	15.4	1.35	770
16	110	150	15.3	1.77	720
17	120	180	15.1	1.36	540

The average loaf volume given by the pastry flour (9.3% protein) was 495 cc. A standard household flour (12.8% protein) gave an average volume of 760 cc. An average loaf volume of 785 cc. was obtained by addition of freeze-dried gluten in the same way as the spray-dried gluten was added.

drying air temperatures. Although there is a good deal of variability in the moisture content of the products, the values are in general agreement with the value of about 2.5% reported by Lusena and Adams (4). Most of the preparations contained less than 2% moisture and only one sample exceeded 3%. No consistent relation existed between the moisture content of the products and any of the variables measured.

Throughout the whole series of experiments on A and B fractions the average difference between the volumes of duplicate loaves was 38 cc., and since most of the volumes reported in Table I fall within a 100 cc. range, the method as

**One hundred grams flour, 4 gm. skim milk powder, 3 gm. fat, 3 gm. yeast, 5 gm. sugar, 1.75 gm. salt, 0.1 gm. $NH_4H_2PO_4$, 1 ml. malt solution (60 gm. non-diastatic malt in 200 ml.).*

used is evidently limited as a means for distinguishing between the preparations.

It is apparent however from the data given that gluten retaining an appreciable amount of its baking quality was obtained over a fairly wide range of conditions. A product comparable to freeze-dried gluten was obtained by operating the drier with an inlet temperature of from 160° to 170° C. and an outlet temperature from 80° to 90° C. Conditions within this range consistently gave a good product and were used for 12 preparations giving loaf volumes in excess of 800 cc. The most severely damaged sample was made with an inlet temperature of 180° C. and an outlet temperature of 120° C. The trends suggest however that an inlet temperature of 180° C. could be used with an outlet temperature below 100° C. Results with these conditions are not reported because with the high flow rate required, severe clogging of the nozzle was encountered. It is significant, however, from a practical point of view, that some of the best products were made with the drier operating near maximum capacity. The deleterious effect of heat above 100° C. was also shown by heating freeze-dried gluten for one hour. Baking tests showed incipient damage at 100° C. followed by a linear decrease in loaf volume from 100° C. to 160° C. At the latter temperature destruction of baking strength was complete.

Fig. 1 contains photographs of the loaves obtained from preparation 6

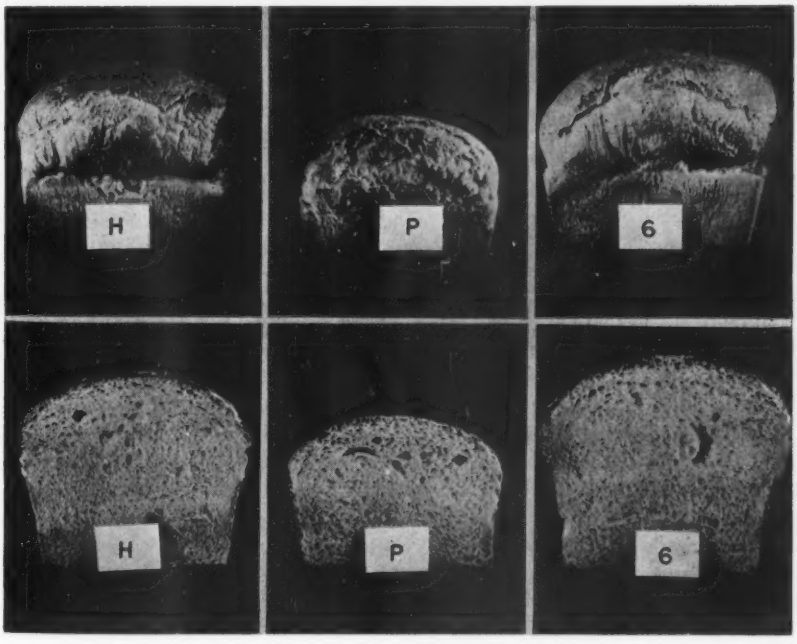

FIG. 1. Comparison of loaves baked from household flour, pastry flour, and pastry flour with spray-dried gluten added.
H—household flour; P—pastry flour; 6—pastry flour plus spray-dried gluten preparation 6.

(Table I) together with those prepared from household flour and pastry flour. Although the loaves shown were somewhat larger than average, they were typical in appearance to those baked with the added gluten and could not be distinguished in appearance from those baked with added freeze-dried gluten. The crust color and shape with preparation 6 was as good as with household flour. In general, loaf characteristics such as crust color and shape were somewhat better for loaves of larger volume. All loaves containing spray-dried gluten were however slightly "overaged". It should be noted that no oxidizing or reducing agents were added to the experimental doughs.

Since the costs of preparing spray-dried gluten would depend on the concentration of solids in the dispersions, some experiments were made with different concentrations of gluten. Standard methods of preparing the solutions were used except that the final volume of dispersing liquid was varied to give the concentration desired. Drying was done with an inlet temperature of 160° C. and an outlet temperature of 90° C. Dispersions containing 3.5, 6.0, 7.0, 8.0, and 11.0% solids gave average loaf volumes of 815, 775, 810, 770, and 775 cc. respectively. The results show no appreciable differences between the various preparations. It seems probable therefore that solutions containing at least 11% solids can be dried satisfactorily. Although concentrations greater than 11% were not tested it appears that such dispersions could be dried without damage if the atomizing system of the particular drier used was capable of producing the necessary uniform fine spray from the somewhat more viscous material.

Baking Characteristics of Spray-dried Gluten

Experiments were done to evaluate more fully the baking strength of spray-dried preparations obtained under optimum drying conditions. Gluten dispersions prepared in the usual way from a straight run flour,* containing 14.5% protein and 0.042% ash, were dried with an inlet air temperature of 160° C. and outlet temperature of 90° C. Using a cake flour containing 7.3% protein as a base, samples of the A fraction were added to give a series of flours ranging from 7.3% to 22% protein (14% moisture basis). Results of baking tests on these are given in Fig. 2. The straight line was calculated from experimental points by the method of least squares. Application of conventional statistical methods gives a regression coefficient, for loaf volume on per cent protein, of 48.2 with a standard error of 1.84. The standard deviation of the loaf volumes from the regression is 32.2 cc.

The regression coefficient of 48.2 indicates good baking quality and compares favorably with results of Aitken and Geddes (1), who, using dried glutens, reported values ranging from about 30 to 59 depending upon the baking formula used. Although Aitken and Geddes obtained an average coefficient of 30.7 without addition of bromate, preliminary experiments in the present investigation indicated that no improvement was obtained upon addition of oxidizing or reducing agents.

**Supplied by Robin Hood Mills, Saskatoon, Sask.*

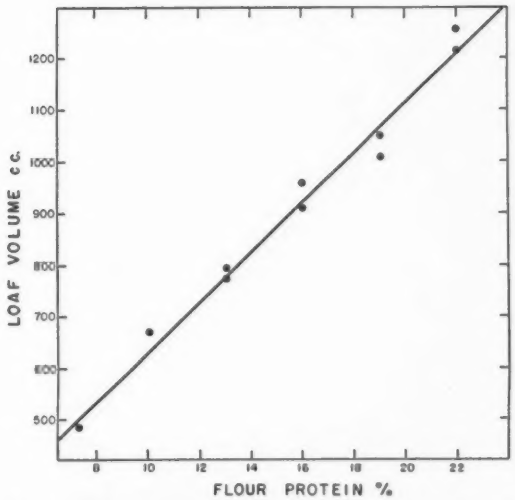

FIG. 2. The effect on loaf volumes of adding spray-dried gluten to a 7.3% protein cake flour. (Regression coefficient for loaf volume on per cent protein = 48.2±1.8. Standard error of loaf volume 32 cc.)

Comparison of Spray-dried Gluten with a Commercial Vital Gluten

The baking behavior of spray-dried gluten was compared with that of a commercially available gluten (hereinafter called vital gluten) of the type used in some dietetic breads. Results with cake flour, raised arbitrarily to 15% and to 40% protein levels by supplementation with the gluten preparations, are given in Table II.

At the 15% protein level results with spray-dried gluten are similar to those presented earlier; however loaf volumes with "vital gluten" were below 600 cc. The loaves were hard and stiff textured and would be quite unacceptable for human consumption. At the 40% protein level, "vital gluten" gave the most acceptable loaves. Those from spray-dried gluten were open textured, soft and gummy, and had volumes greater than 2000 cc.

TABLE II

COMPARISON OF FLOURS SUPPLEMENTED AT TWO LEVELS WITH DRIED GLUTENS

Composition of flours	Protein content, % (14% moisture)	Average loaf volume, cc.	Comments
Cake flour only	7.3	420	
Cake flour + "vital gluten"	15.0	580	Stiff texture, gray color
Cake flour + spray-dried gluten	15.0	800	Even texture, good loaf
Cake flour + "vital gluten"	40.0	710	Smooth texture, brownish color
Cake flour + spray-dried gluten	40.0	Over 2000	Very open texture, soft, and gummy under pressure

Although spray-dried gluten evidently is not suitable for preparation of protein-rich bread, the results shown in Table II are another demonstration of its baking strength. Using the volumes at 7.3% protein and 15% protein, a regression coefficient of 49 is estimated. (See Fig. 2.) If the linear relation between protein content and loaf volume holds over a wide range of concentrations, the volume expected at 40% protein would be 2020 cc. This is consistent with the estimated volumes above 2000 (Table II).

Water Vapor Adsorption by Dried Gluten

In connection with problems of packaging and storage, water vapor adsorption by gluten at different humidities was investigated using apparatus as described by Colvin, Craig, and Sallans (2). Humidifying columns thermostated at 25° C. were used to condition the atmosphere for 1-gm. samples of previously dried gluten. Air of controlled humidity was passed over the samples at the rate of 360 ml. per hour until moisture equilibrium was obtained (indicated by constant weight). Four to five days were usually required for this.

The results in Table III show a pattern of moisture adsorption typical of plant materials (2) and suggest that dried gluten will adsorb some moisture

TABLE III

EQUILIBRIUM MOISTURE CONTENT OF GLUTEN AT VARIOUS RELATIVE HUMIDITIES (% BY WT.)

Relative humidity of air, %	Saturated salt solution in humidifying column	Equilibrium moisture content, %			
		Spray-dried gluten		Freeze-dried gluten	
		Sample 1	Sample 2	Sample 1	Sample 2
11	LiCl	5.5	4.0	4.5	3.9
33	$MgCl_2$	6.9	7.4	5.4	7.6
52	$Mg(NO_3)_2$	12.0	10.0	9.4	10.1
75	NaCl	13.4	14.7	12.9	17.1
93	KNO_3	17.9	18.8	18.7	16.5

from the atmosphere even when stored at relative humidities as low as about 10%. At humidities of 93%, the samples became wet in appearance and tended to shrink to a gummy mass. The uptake of moisture even at fairly high humidities is however not excessive and under ordinary conditions would not likely give rise to serious difficulties in storage and packaging.

Microscopic Examination of Spray-dried Gluten

To further characterize the spray-dried glutens, photomicrographs of a number of preparations were made. From these, estimates of the particle size and size distribution were obtained. Fig. 3 shows typical photomicrographs of spray-dried gluten and of household flour. Photograph A shows that the powder particles are spherical in shape and not greatly variant in size. A number of particles appeared as hollow spheres with "vapor" holes in their

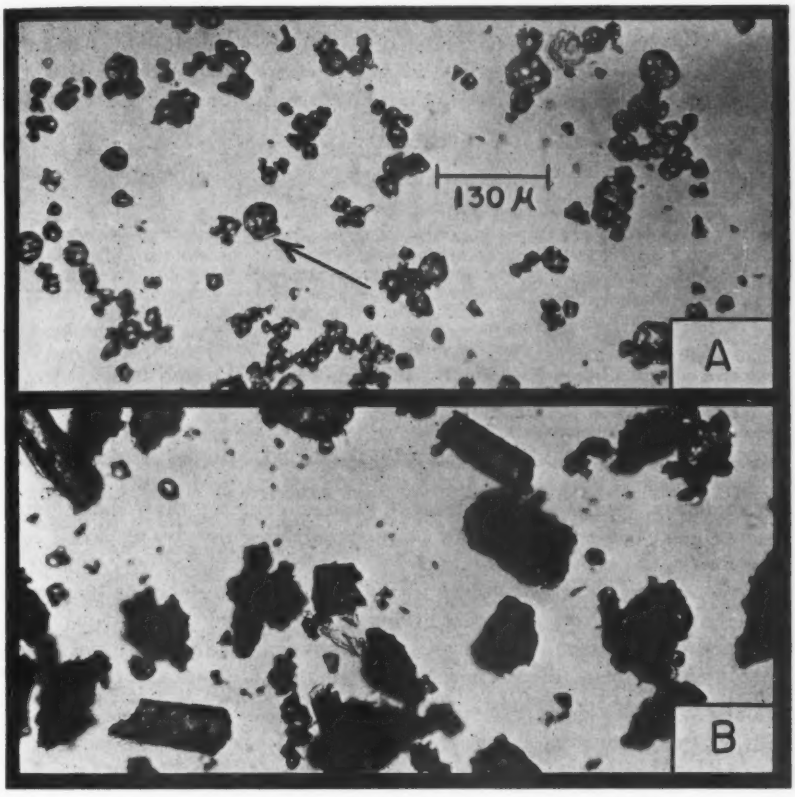

FIG. 3. Photomicrographs of some spray-dried glutens and of household flour.
A—spray-dried gluten; B—household flour.

side (see arrow). The hollow spheres are characteristic of many spray-dried materials (5).

An estimate of the particle size distribution in some spray-dried gluten preparations was obtained by scaling 100 randomly selected diameters on photomicrographs. Between 50 and 60% of the particles were between 10 and 20 microns in diameter. In most samples 20% or more of the particles were less than 10 microns in diameter and although there were always some of larger size, there were very few with diameter greater than 40 microns. Photomicrograph A was chosen to show the appearance of the particles rather than their size distribution.

The relative fineness of the gluten suggests that it should be uniformly distributed throughout the flour by dry mixing (compare photomicrograph B), and indicates that little would be gained, as far as uniform reincorporation of gluten is concerned, by smaller particle size.

Summary of Properties of Spray-dried Gluten

Table IV is a summary of characteristics of spray-dried gluten. The almost complete dispersibility in acetic acid is in accord with evidence that the physical characteristics of gluten are not extensively altered by its separation and spray drying.

TABLE IV

SOME PROPERTIES OF SPRAY-DRIED GLUTEN

Nitrogen content	15.4%±0.3%
Moisture content as prepared	0.4% to 4%
Equilibrium moisture content:	
Relative humidity 33%	7%
Relative humidity 75%	14%
Bulk density (flour 0.6)	0.17±0.03
Per cent of total nitrogen dispersible in 0.01 *N* acetic acid (8% solids)	99.4
Regression coefficient:	
Loaf volume over % gluten added	48
Median particle diameter (av.)	18 microns

In summary, results presented herein provide evidence that wheat gluten retaining good baking quality can be prepared by spray drying acetic acid dispersions of the protein. Since a good product was obtained over a range of drying conditions, it would appear that, with the more efficient large-scale drying units, satisfactory control of drying variables could be readily achieved. The experimental data presented on several physical characteristics of spray-dried gluten may be of interest when considering the utilization of the material or the problems of its packaging and storage.

ACKNOWLEDGMENTS

The test baking reported in this work was done in the baking laboratory of the University of Saskatchewan. For this the author is indebted to Dr. E. Y. Spencer, now of the Science Service Laboratory, London, Ontario, Dr. C. Walden, Cereal Chemist, now of British Columbia Research Council, and Mr. R. Teed, baking technician, University of Saskatchewan. The author is also indebted to Dr. H. R. Sallans for helpful suggestions, to Mr. K. L. Phillips for engineering assistance, and to Mr. W. Sauder for technical assistance.

REFERENCES

1. AITKEN, T. R. and GEDDES, W. F. Cereal Chem. 16: 223–231. 1939.
2. COLVIN, R., CRAIG, B. M., and SALLANS, H. R. Can. J. Research, F, 25: 111–118. 1947.
3. LUSENA, C. V. Cereal Chem. 27: 167–178. 1950.
4. LUSENA, C. V. and ADAMS, G. A. Cereal Chem. 27: 186–188. 1950.
5. MARSHALL, W. R., Jr. and SELTZER, E. Chem. Eng. Progr. 46: 501–508. 1950.
6. PRATT, H. K. and YAMAGUCHI, M. Science, 112: 560–561. 1950.
7. WOODCOCK, A. H. and TESSIER, H. Can. J. Research, A, 21: 75–78. 1943.

HUMIDIFICATION OF COLD STORAGES: THE JACKET SYSTEM[1]

By C. P. Lentz

ABSTRACT

Basic principles of the jacket system of maintaining high relative humidity in cold storages are outlined. Drying by the cooling coil is prevented by circulation of the refrigerating air stream through a jacket surrounding the room rather than through the room. Relative humidities between 89 and 98% were maintained in the test room, the level depending mainly on rate and direction of air circulation in the jacket and on air flow resistance. Spatial variations in room temperature were less than 2° F. during most tests and velocity of air movement was negligible. Reduced frosting of the cooling coils in jacketed systems may offset most of the 10–15% increase in operating cost resulting from the increased air circulation required. The application of the test results in the design of jacketed storage rooms is discussed.

INTRODUCTION

The use of a jacketed storage room was first proposed by A. G. Huntsman in 1931 as a means of reducing surface desiccation of frozen fish (2). Tests reported by Huntsman showed that drying in the room he designed was reduced to one-fifth of that occurring in conventional storage rooms. Further work on the jacketed system was reported by O. C. Young in 1933 (5). His work showed that uniform temperatures could be maintained in a jacketed room, and emphasized the importance of an effective vapor seal between the room and the jacket air space. This type of room, with its uniform temperature and high relative humidity, would appear to have a marked advantage over conventional rooms in the storage of most frozen foods. Although a number of jacketed storages have been built, the principle has not been applied extensively, presumably because of the lack of generally applicable design and operating information. This paper reports an investigation made to obtain such information.

Principle of Operation of the Jacket System

Surface desiccation is caused mainly by the migration of moisture from the surface of the stored product to the refrigerating surface, the rate of desiccation being proportional to the difference in vapor pressure between produce surface and refrigerating surface. In the jacketed system the refrigerating air circulates through a jacket or system of ducts entirely surrounding the room, rather than through the room itself (Fig. 1). Hence, the difference in vapor pressure between product and refrigerating surfaces is not directly dependent on the external heat load or the operation of the refrigeration system.

If no heat or moisture is given off or absorbed in the room and if temperatures in the jacket remain constant, the equation

$$Q = WC(t_2 - t_1) ,$$

[1]*Manuscript received March 24, 1955.*
Contribution from the Division of Applied Biology, National Research Laboratories, Ottawa. Issued as N.R.C. No. 3630.

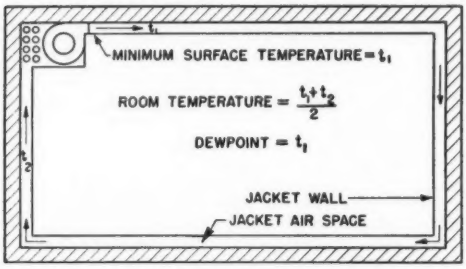

FIG. 1. Schematic sketch of jacketed room.

where Q = heat transferred into room through insulation,
W = weight of air circulated through jacket,
C = specific heat of air,
t_1 = temperature of air entering jacket,
t_2 = temperature of air leaving jacket,

can be used to explain the operation of the system. If air flow distribution in the jacket is uniform, the room temperature will be $(t_1 + t_2)/2$ and if the inside wall of the jacket is vapor-proof but without thermal resistance the lowest surface temperature and dewpoint of the air in the room will be t_1. For a given Q, it is apparent that the relative humidity in the room will depend on W, the amount of air circulated through the jacket.

In practice, the relative humidity in the room may be affected by variations in the temperature of the air in the jacket, uneven distribution of the circulating air, and heat loads in the room. Since these factors determine the amount of air that it is practical to circulate in the jacket, they will be considered separately.

(*a*) *Temperature Variations in Jacket Air*

Temperature variations in the jacket tend to reduce the humidity in the room. The magnitude of the effect depends on the amplitude and period of the variations, and on the thermal inertia of the inner wall of the jacket. As pointed out by Young (5) the use of some thermal insulation in the jacket wall (e.g. $\frac{3}{4}$ in. wood sheathing) will reduce the effect of temperature cycling of the jacket air.

(*b*) *Heat Loads in the Room*

The effect of heat loads in the room is to raise the room temperature above $(t_1 + t_2)/2$, and hence to lower the relative humidity. Heat transfer into the room from the jacket has a similar effect. Since there is a temperature gradient in the jacket air (t_1 to t_2), heat will flow into the room through the warmer surfaces, and out through the colder surfaces. If the inner jacket wall has no thermal resistance, the coldest part of the wall surface will be t_1 and the warmest part t_2. Insulation will reduce the heat flow and hence lower the warmest surface temperature and raise the coldest surface temperature.

Heat transfer into the room through the structural members in the jacket air space is also reduced by this insulation.

(c) Air Flow Distribution in Jacket

Uneven air flow distribution in the jacket will act in two ways to reduce the relative humidity. First, additional heat will be transferred into the room from parts of the jacket having reduced flow, and second, the area through which heat is transferred out of the room and into the jacket will be reduced. Both of these factors tend to increase the difference between the room temperature and the temperature of the coldest part of the jacket wall, and hence to lower the relative humidity. It can be seen that if temperature variations and uneven flow distribution in the jacket result in a room temperature 5° F. above the coldest wall surface temperature, there is slight advantage in circulating enough air to reduce $(t_2 - t_1)$ to 1° F.

APPARATUS AND PROCEDURE

Description of Test Room

The test room (Fig. 2) was constructed so that the results obtained could

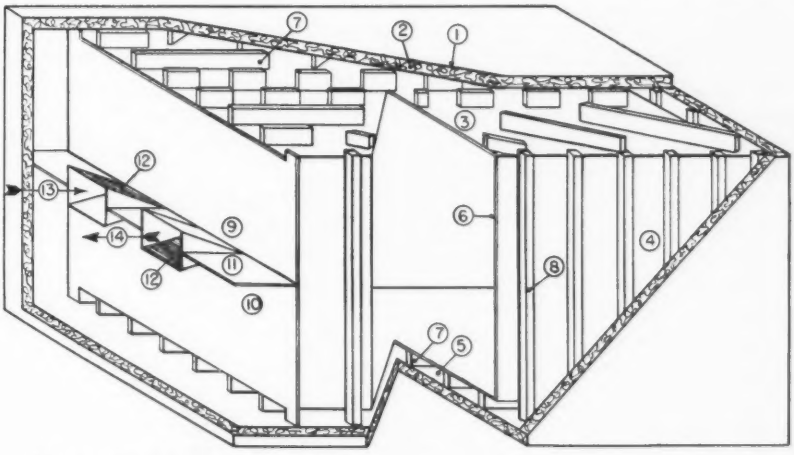

FIG. 2. Cut-away view of jacketed test room.
(1) Vapor barrier.
(2) Mineral wool insulation 8 in. thick.
(3) Ceiling air space.
(4) Wall ducts.
(5) Floor air space.
(6) Insulated and vapor proof inside wall (asphalt painted plywood over "Ten-test" ½ in. thick).
(7) Ceiling and floor air guides, 6 in. deep.
(8) Wall air guides, 2½ in. deep.
(9) Top plenum chamber.
(10) Bottom plenum chamber.
(11) Horizontal partition.
(12) Dampers to change direction of air circulation.
(13) Air in.
(14) Air out.

be applied readily in the design of commercial storages. The inside dimensions of the room were 10 × 10 × 20 ft. long. The system was designed so that air could be circulated through the jacket from top to bottom or from bottom to top at any rate desired. The jacket ducts were constructed so that uniform flow would be obtained in the walls rather than in the entire jacket. This was done by reducing the depth of the ducts in the walls compared with those in the floor and ceiling, and thus increasing the proportion of the total friction pressure loss occurring in the walls. Since ideal distribution requires the quantity of air flowing in each circulation path to be proportional to the length of the path, the design used represents a compromise in the interest of practical simplicity. The inside wall of the jacket was insulated and vapor-proofed for reasons already mentioned.

Accurate temperature control was obtained by maintaining a constant ambient temperature and by heating the air entering the jacket to eliminate the effects of changes in refrigeration capacity.

Measurements

Temperatures were measured with thermocouples installed so that conduction errors would be minimized. Twenty-seven elements were located in the room air, seven in the jacket air, and ten were attached to the inside surface of the room. The surface thermocouples were placed in areas of maximum and minimum surface temperature. In addition, fourteen differentially connected couples were used to measure temperature differences between top and bottom of wall ducts. Variations in flow distribution in the ducts were estimated from these differences.

Relative humidity was measured at five locations in the room by the wet- and dry-bulb method. This method had been found to give satisfactory results in an earlier investigation (3). Each instrument consisted of a dry-bulb thermocouple and a series of ten differentially connected wet- and dry-bulb junctions. The measurements were checked by the gravimetric method using chemical absorption. Relative humidity was calculated with reference to the vapor pressure of ice since this is the datum of interest in frozen food storage.

Velocity and static pressure measurements were made with a micromanometer and Pitot tube. Air flow rates were calculated from velocity pressure measurements made in an orifice in the inlet to the jacket plenum chamber (Fig. 2). Jacket friction pressure loss was calculated from the pressure difference between the top and bottom sections of the plenum chamber.

Scope of Tests

The effects of jacket air flow rate, duct friction pressure loss, and forced air circulation in the room were studied with both top-to-bottom and bottom-to-top circulation in the jacket. The rate of air flow in the jacket was varied to give differences in temperatures of 1 to 10° F. between the air entering and leaving the jacket. This range includes the entire range likely to be of interest in storage practice. The effect of duct resistance was studied after preliminary tests indicated the importance of this variable. This resistance was varied by

partially closing the dampers in the wall ducts. Tests were also made using forced circulation in the room because such circulation may be necessary in practice when produce must be cooled quickly. The amount of circulation during these tests was approximately equal to that in comparable rooms using forced air cooling units. In addition, two tests were made to determine the value of insulating the jacket wall. In one of these, the temperature of the air entering the jacket was varied through a ±4° F. cycle in four hours and in the other a heat source equal to half the external heat leakage was put in the room.

The room was empty and at a temperature of 0° F. for all of the tests. The room was not loaded because the thermal inertia of a load would have decreased the sensitivity of the room to changes in operating conditions. Other temperatures were not tested because the performance of the room at one temperature can be used to predict its performance at other temperatures.

Most of the tests were continued for two or three days after constant temperatures were reached. Several longer tests (two weeks) were made to ascertain whether or not any slow changes were taking place. In all, the jacketed room was operated for more than a year.

RESULTS

Relative Humidity

Relative humidity in the room varied with rate and direction of air circulation in the jacket, decreasing from 98% at high rates of circulation to 89% with a low rate of flow in the top-to-bottom direction (Fig. 3). The decrease was gradual with bottom-to-top circulation and did not exceed 2% at the lowest rate of flow tested. With top-to-bottom circulation the relative humidity dropped sharply as the flow rate was reduced below 1200 c.f.m. This critical circulation rate was reduced by partial closure of the wall ducts with dampers. The dampers had little effect with bottom-to-top circulation.

Since the dewpoint in the room was higher than the lowest wall surface temperature during most of the tests, relative humidities based on minimum surface temperature (Fig. 4) are lower than the actual relative humidities measured (Fig. 3). This discrepancy was caused by the slow migration (from warmer to colder wall surfaces) of moisture deposited on all surfaces during door openings. Since the dewpoint temperature in the room would eventually equal the lowest surface temperature, the calculated relative humidities are a better criterion of performance than those obtained by the wet-bulb method. Top-to-bottom circulation gave the best results on the basis of minimum surface temperature.

Air Movement in the Room

Smoke tests showed that air velocities in the jacketed room were negligible (less than 5 f.p.m.) under all conditions tested.

Forced air circulation in the room reduced relative humidities calculated from wet-bulb measurements (Fig. 3) but had no appreciable effect on those based on minimum surface temperature (Fig. 4). Since earlier experiments (3)

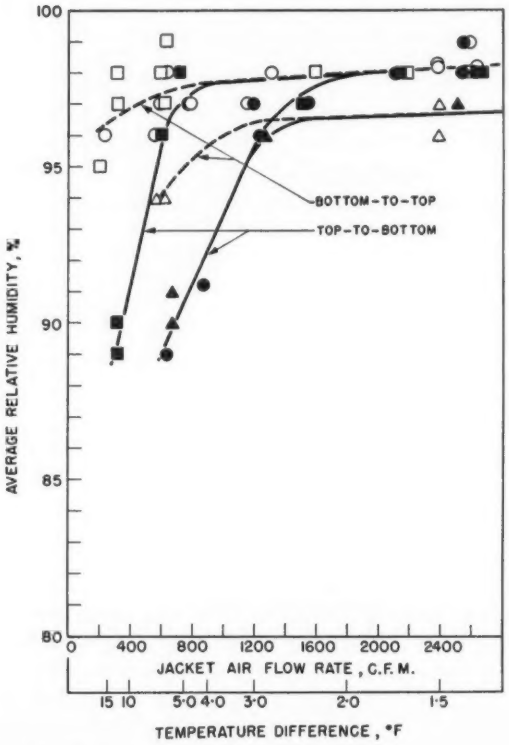

FIG. 3. Relative humidity based on wet-bulb depression.
● ○ Ducts open. ■ □ Ducts partially closed. ▲ △ Forced circulation in room.
Closed symbols: top-to-bottom circulation. Open symbols: bottom-to-top circulation.
Note: (1) For approximate air velocity in wall ducts divide c.f.m. by 10 (Figs. 3–7 incl.).
(2) "Temperature difference" refers to increase in temperature of air in circulating through jacket (Figs. 3–7 incl.).

showed that similar changes in air velocity (5 f.p.m. to 100–300 f.p.m.) did not cause error in the wet-bulb depression, the results indicate that forced air circulation decreased the dewpoint of the room air. The decrease may have been caused by a proportionally greater increase in the rate of condensation than in the rate of evaporation of migrating moisture.

Spatial Temperature Variations

Spatial variations in room temperature were larger with bottom-to-top circulation than with top-to-bottom circulation (Fig. 5). The critical rate of air flow indicated by the relative humidity measurements is also shown by the temperature variations. Variations in dewpoint temperature (calculated from wet-bulb measurements) were similar to those in the dry-bulb temperatures. The dewpoint variations are of no consequence in assessing the performance

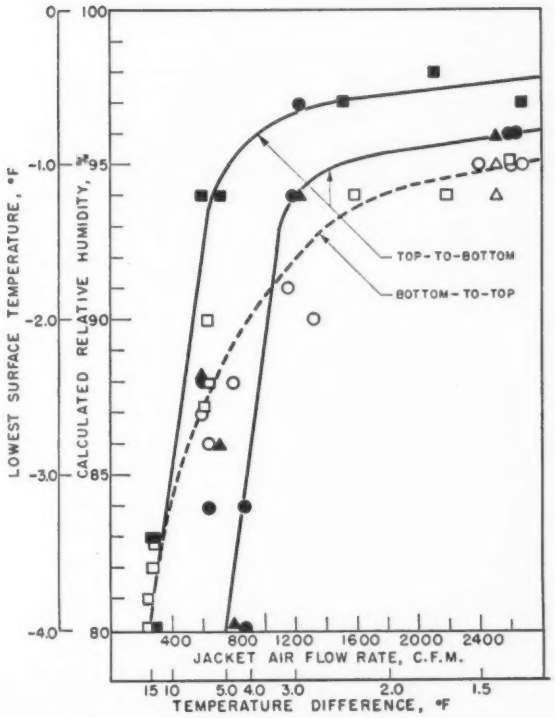

FIG. 4. Relative humidity based on lowest surface temperature.
● ○ Ducts open. ■ □ Ducts partially closed. ▲ △ Forced air circulation in room.
Closed symbols: top-to-bottom circulation. Open symbols: bottom-to-top circulation.

of the room, however, since the door openings causing these variations would not have appreciable effect in practice.

Jacket Temperatures and Friction Pressure Loss

The average jacket temperature was approximately the same for top-to-bottom and bottom-to-top circulation at high rates of flow (Fig. 6). As the rate of flow with top-to-bottom circulation was decreased below the apparently critical rate, the average jacket temperature dropped sharply. Temperature differences in the wall ducts indicated that the change in operating characteristics was due to non-uniform air flow distribution in the ducts. At the critical flow rate the direction of circulation in some of the ducts apparently reversed and the number of ducts with reversed circulation increased as the rate of circulation was further reduced. Calculations based on duct air temperatures showed that differences in density due to differences in temperature between ducts were sufficient to reverse the direction of circulation at these low rates of flow. Increases of 10–15° F. in surface temperatures in some locations gave further evidence of poor circulation. It may be noted that the difference

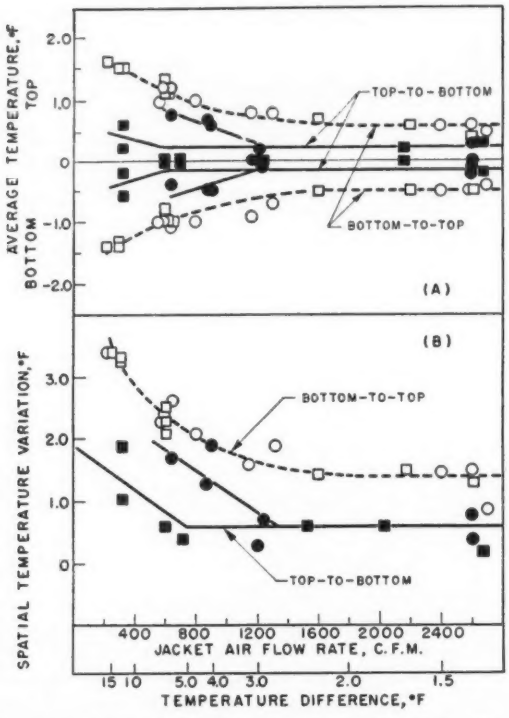

FIG. 5. Spatial temperature variation in test room. (A) vertical, (B) maximum.
● ○ Ducts open. ■ □ Ducts partially closed.
Closed symbols: top-to-bottom circulation. Open symbols: bottom-to-top circulation.

between the average jacket temperature $(t_1 + t_2)/2$ and the average room temperature (0° F.) is a measure of the amount of heat flowing into the room through the jacket and its structural members.

Friction pressure loss in the jacket was doubled (Fig. 7) by partial closure of the wall duct dampers to improve air flow distribution in the jacket. Even at high rates of flow, however, the friction pressure loss in the jacket was not significant when compared with the pressure loss in the evaporator and fan (0.5 in water).

Temperature Cycling and Heat Load Tests

During the temperature cycling tests the room temperature varied one-third as much as the jacket temperature. It should be noted that the variation in room temperature would be even smaller for cycles of shorter period.

A heat load of 2000 b.t.u./hr. raised the room temperature 5.7° F. This is approximately the amount the same heat load would raise the temperature of a comparable room cooled by a forced air circulation evaporator operating continuously with a 10° F. refrigerant-room air temperature difference.

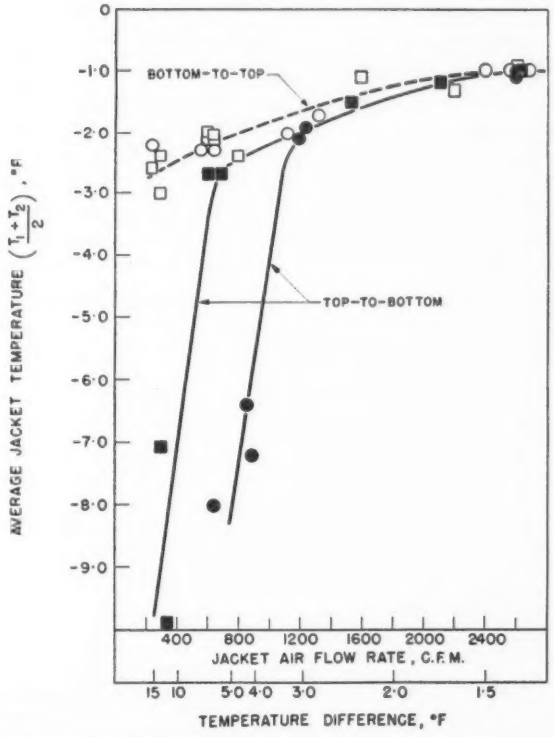

FIG. 6. Average temperature of air in jacket.
● ○ Ducts open. ■ □ Ducts partially closed.
Closed symbols: top-to-bottom circulation. Open symbols: bottom-to-top circulation.

DISCUSSION

Relation of Operating Characteristics to Jacket Air Circulation

Relative humidity, minimum surface temperature, and spatial temperature variations in the room depended on the rate and direction of air circulation in the jacket. With bottom-to-top circulation these variables changed at an approximately uniform rate as the rate of air flow was changed. With top-to-bottom circulation there appeared to be a critical rate of flow below which changes occurred more rapidly. The critical rate of flow appeared to depend on flow resistance. These characteristics of the room can be explained by considering the effect of two factors on the operation of the system. These factors are the constant rate of heat flow into the jacket air space, and the differences in flow resistance between air flow paths in the jacket. Less air flows in those paths having higher resistance than others. Since the same amount of heat is absorbed in each of the wall ducts, the average temperature in the ducts with lower rates of flow will be higher than in others. With bottom-to-top circulation, the resulting differences in density between ducts tend to

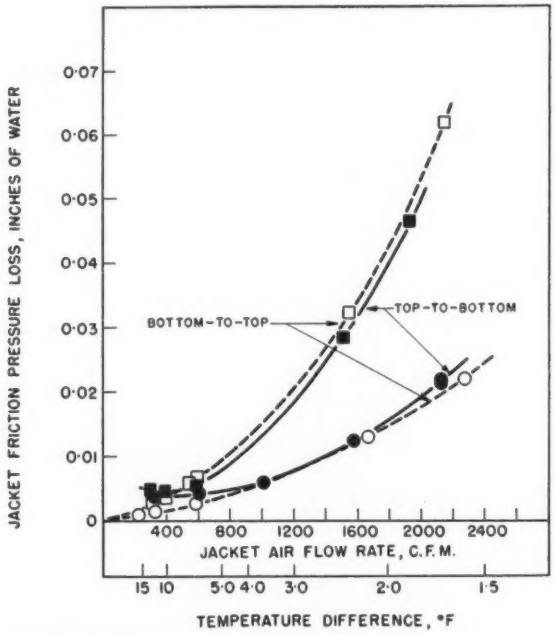

FIG. 7. Friction pressure loss in jacket.
● ○ Ducts open. ■ □ Ducts partially closed.
Closed symbols: top-to-bottom circulation. Open symbols: bottom-to-top circulation.

maintain uniform flow. With top-to-bottom circulation, however, these differences in density tend to increase differences in flow. When the pressures due to differences in density approach the friction pressure loss (Fig. 7), flow becomes unsteady and may reverse in direction. The resulting poor distribution of refrigerating air in the jacket increases spatial temperature variations in the jacket and the room, and hence, lowers relative humidity.

Design of Jacketed Rooms

If allowance is made for changes in dimensions, insulation, and temperature conditions, the results obtained with the test room should be generally applicable in the design of jacketed rooms. Although the jacketed room represented an improvement over most directly cooled rooms with all of the types of operation tested, the results showed that direction and rate of air circulation, duct design, and jacket wall construction affected conditions in the room significantly. Each of these factors will be considered separately.

(*a*) *Direction and Rate of Air Circulation*

With good distribution of flow in the ducts, top-to-bottom circulation gave higher minimum surface temperatures and smaller spatial temperature variations than bottom-to-top circulation (Figs. 4 and 5). The resulting difference

in rate of surface desiccation would be increased by forced circulation in the room. It may be noted that the advantage of top-to-bottom circulation depends on uniform circulation in the jacket. With poor construction, or insufficient circulation, bottom-to-top circulation could give better results.

The rate of air circulation required depends mainly on the conditions desired and on the heat load to be absorbed. The results indicate that 1000 c.f.m. would be the minimum satisfactory rate in the test room and that little would be gained by increasing the circulation rate above 1800 c.f.m. These limits correspond to temperature differences of 4 and 2° F. respectively, between the air entering and leaving the jacket. The cost of fan and refrigeration power should also be considered. Since lower jacket temperatures require lower refrigerant temperatures, the cost of refrigeration power increases as the rate of circulation is reduced. Fig. 8 shows that the cost of fan power increases

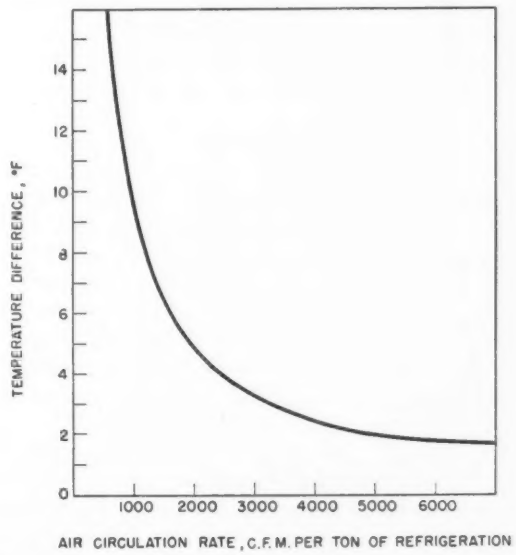

FIG. 8. Relation between jacket temperature difference and air circulation rate.

rapidly as the jacket temperature difference is reduced below 2° F., and the refrigeration power increases rapidly as the rate of air circulation is reduced below 1200 c.f.m. per ton, on a sensible heat basis.

(*b*) *Duct Design*

The main object of the jacket ducts is to distribute air through the jacket in proportion to the heat to be absorbed. For top-to-bottom circulation a practical design appears to be one in which the friction pressure loss in the wall ducts is uniform, represents a large proportion of the total friction pressure loss in the jacket, and is appreciably larger than the pressure differ-

ences due to differences in density between ducts. Increasing the duct resistance in the test room improved its operation, and the results indicate that further increase in resistance would have given further improvement. The maximum resistance that may be used depends only on cost of fan power. In the test room the resistance of the jacket at the critical rate of flow was less than 0.01 in water. Since this represents less than two per cent of the pressure loss normally occurring in evaporator-and-fan systems, it could be increased by a factor of 5 to 10 without causing a prohibitive increase in fan power. Increased resistance should be obtained by using smaller ducts rather than greater flow, because greater flow also increases pressure loss across the evaporator. Fig. 9 shows that the test room should have been designed with ducts 1–1½ in. deep instead of 2½ in. deep.

The minimum permissible flow resistance is less easily decided because it

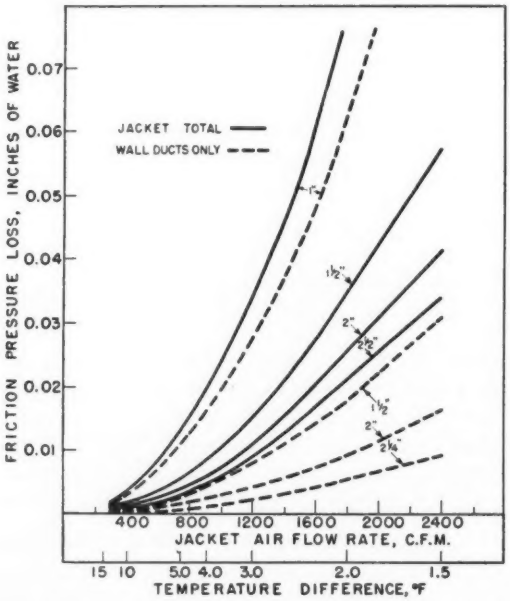

FIG. 9. Calculated friction pressure loss in jacket for wall ducts 1, 1½, 2, and 2½ in. deep.
Note: (*a*) For approximate air velocity in wall ducts 2½ in. deep divide c.f.m. by 10, velocities in other wall ducts inversely proportional to duct depth.
(*b*) Assumptions made in calculations:
1. Jacket and wall duct entrance loss = 0.5 v.p.
2. Jacket and wall duct exit loss = 1.0 v.p.
3. Area of jacket entrance and exit = 5 sq. ft.
4. Cross-sectional area of wall ducts 2½ in. deep = 11 sq. ft.
5. Friction pressure loss in floor and ceiling jacket negligible, except for entrance and exit losses.
6. Absolute roughness of jacket surfaces 0.05 in.
7. The basic flow equation for circular ducts is applicable to the circular equivalents of the wall ducts.

depends mainly on the variation of flow resistance in the ducts, which is a function of materials and construction, as well as design. Wall height and the ratio of air circulated to heat absorbed also affect the minimum pressure loss which will give satisfactory operation. A higher rate of heat absorption gives larger temperature differences and hence larger differences in density and pressure. Although both friction pressure loss and pressure difference due to difference in density are proportional to duct height, allowance should be made for duct height because of the proportion of the duct resistance represented by entrance and exit pressure losses. The minimum permissible loss should cause no difficulty in design however, since a liberal factor of safety can be allowed without appreciable increase in cost. In addition, friction pressure loss can be adjusted with dampers if necessary.

(*c*) *Jacket Wall Construction*

The main requirements of the jacket wall are that it be a good water vapor barrier, and that it have some thermal resistance, as already discussed. The amount of insulation which should be used depends on the conditions desired. For most purposes the insulation used in the test room would be adequate.

CONCLUSION

The results of this study indicate that surface desiccation of frozen products during storage can be reduced to negligible levels by use of the jacketed room. Not only can relative humidities approaching 100% be maintained, but the uniform temperatures and low air velocities in the room should reduce surface desiccation to levels much below those which would occur in directly cooled rooms at similar levels of relative humidity.

In addition to reducing surface desiccation of stored produce, the jacketed room offers a solution for the problem of deterioration of insulation resulting from moisture condensation. This problem is particularly serious where the vapor pressure and concentration gradients periodically reverse in direction. Moisture condensation in insulation was discussed by Munters (4) who suggested the circulation of dry air through the insulation.

The operating cost for a jacketed room may not be much higher than for a comparable directly cooled room. Although the increased air circulation required for jacketed operation increases power consumption by 10–15%, this increase in cost may be more than offset by the increased efficiency of operation of the evaporators that results from reduced frosting.

In the jacketed system high relative humidity is maintained by preventing moisture from leaving the room. Since this method is not effective where there is moisture absorption in the room, moisture absorption by packaging materials may cause appreciable surface desiccation. Such absorption would not be a problem in a system in which high relative humidity is maintained by moisture addition (as in the direct humidification system described earlier (1, 3). The answer to the problem may be provided by a combination of the two systems now being studied.

ACKNOWLEDGMENT

The author wishes to thank Mr. E. A. Rooke, in particular, for assistance in the design and construction of the test facilities, as well as in making the tests.

REFERENCES

1. Cook, W. H. Refrig. Eng. 38: 229–233. 1939.
2. Huntsman, A. G. The processing and handling of frozen fish as exemplified by ice fillets. Biol. Board Can., Bull. No. XX: 44–46. 1931.
3. Lentz, C. P. Can. J. Technol. 32: 156–163. 1954.
4. Munters, C. Refrig. Eng. 57: 795–803. 1949.
5. Young, O. C. A jacketed cold storage room. Contribs. Can. Biol. and Fisheries, Vol. VII, No. 39 (Ser. C, Industrial, No. 11): 497–504. 1933.

AUTOMATIC TRANSLATION OF AERATION DATA BETWEEN DIFFERENT FERMENTORS[1]

By Ping Shu

ABSTRACT

The present paper describes an apparatus with which the rate of oxygen uptake of a fermentation conducted in a master fermentor such as shake flask may be automatically duplicated in a slave fermentor, such as a deep tank. The device consists of an element coupling the fermentors and a closed loop aeration control system for the deep tank fermentor. The function of the former is to compare the oxygen uptake rate of the fermentor with that of the shake flask. The function of the latter is to correct the difference in the oxygen uptake rates transmitted from the comparator by regulating the agitator speed of the tank. The agitator speed and the power requirement for such duplication are determined. Hydrogen peroxide is used as a source of oxygen supply for the fermentor and gaseous oxygen for the shake flask; the scale of fermentation may be amplified by varying the hydrogen peroxide concentration. The performance of this translation device was demonstrated with fermentations by *Ustilago zeae* and *Aspergillus niger* cultures. The device offers a solution to the problem of translating the aerations in the event of a change in the scale of a fermentation or the type of the fermentors employed. It also provides a convenient means for direct comparison of the aeration efficiency of different types of fermentors of various sizes under actual fermentation conditions.

INTRODUCTION

Among the nutrients utilized during an aerobic fermentation only oxygen is supplied continuously. The method for controlling its rate of supply varies with the type of the fermentor employed.

In shake flask fermentations, the extent of aeration may be altered by changing either the speed of the shaker or the surface volume ratio of the medium. In the deep tank fermentor, aeration is varied by changing either the stirrer speed or the air flow (2, 9). The relation between these variables and the rate of oxygen transfer through the gas–liquid interface is complicated. It varies with different fermentations and involves such parameters as surface tension, and dissolved and suspended materials.

A convenient sulphite oxidation method was introduced by Cooper *et al.* (3) to establish the relation between stirrer power and rate of oxygen transfer in an aerated tank. This technique has been used by Karow *et al.* (6) to scale up a streptomycin fermentation from 5 liters to 15,000 gal. Wegrich and Shurter (13) scaled a penicillin fermentation from 5 gal. to 24,000 gal. by using stirrer power data alone. Since these procedures do not involve the measurement of the rate of oxygen transfer during actual fermentation, they can only be applied to geometrically similar fermentors. Hixson and Gaden (4), Wise (14), and Bartholomew *et al.* (1) employed a polarographic method to determine the oxygen transfer rate in presence of actively metabolizing organisms. This

[1]*Manuscript received March 31, 1955.*
Contribution from the National Research Council of Canada, Prairie Regional Laboratory, Saskatoon, Saskatchewan. Issued as N.R.C. No. 3629. Presented at the Biochemical Engineering Symposium of the 47th Annual Meeting of The American Institute of Chemical Engineers, New York, N.Y., December 12–15, 1954.

permits the comparison of aeration efficiency of different fermentors under actual fermentation conditions. Recently Hoover *et al.* (5) described a device with which the oxygen concentration in the effluent gas from a fermentor may be continuously recorded by measuring its paramagnetic susceptibility. This offers a more convenient means for studying the aeration problem.

In the development of a fermentation process, it is often necessary to change the size and type of fermentor. For example, shake flasks are commonly used in the initial stage of development and a small tank fermentor at the next stage. It is a difficult problem to find the conditions that will reproduce the magnitude of aeration.

The present paper introduces a device that permits the rate of oxygen uptake of a fermentation in a given fermentor to be automatically duplicated in another fermentor of different size and type. The stirring speed required and the power demand to obtain such aeration are determined. It provides a convenient means of finding the conditions for reproducing the magnitude of aeration in the event of enlargement of the scale of a fermentation or a change in the type of the fermentor employed. Specific examples are given to illustrate the duplication of the oxygen uptake rate of a shake flask fermentation in a deep tank fermentor.

APPARATUS

General Description

To translate the aeration data from one fermentor to another, the fermentation must be done in these two fermentors simultaneously. The rates of oxygen uptake are compared from time to time. Whenever differences occur, the oxygen uptake in one fermentor is adjusted so that it follows that of the other. Conditions to obtain the required magnitude of aeration may then be determined. Fig. 1 shows a schematic diagram of such a system in which a shake flask serves as the master fermentor while the rate of the oxygen uptake is duplicated in a small stirred tank. The closed shake flask system (block *A*) is the same as that described in a previous paper (10) except that the positioning motor only moves the level follower of the oxygen reservoir upward. The apparatus for measuring the oxygen uptake in the tank fermentor (blocks *B* and *D*) is similar except that oxygen is supplied by the catalytic decomposition of hydrogen peroxide. Lead, lead oxide, permanganate, and selenium in fused granules are used as catalysts (7). The decomposition of hydrogen peroxide is instantaneous and quantitative. The amount of water collected in the cylinder is a measure of the volume of hydrogen peroxide consumed.

Air in the fermentor is recycled with a diaphragm pump[2] after it is passed through 30% sodium hydrozide solution. Part of the air is recycled over the top of the fermentor and the rest passes through the medium. The extent of total recycling is adjusted with valve V_2 on the pass shunt across the pump. The rate of air passing through the medium is varied by adjustment of valves V_1 and V_3.

[2]*Dyna-pump, a product of Scientific Glass Apparatus Co., Bloomfield, N.J.*

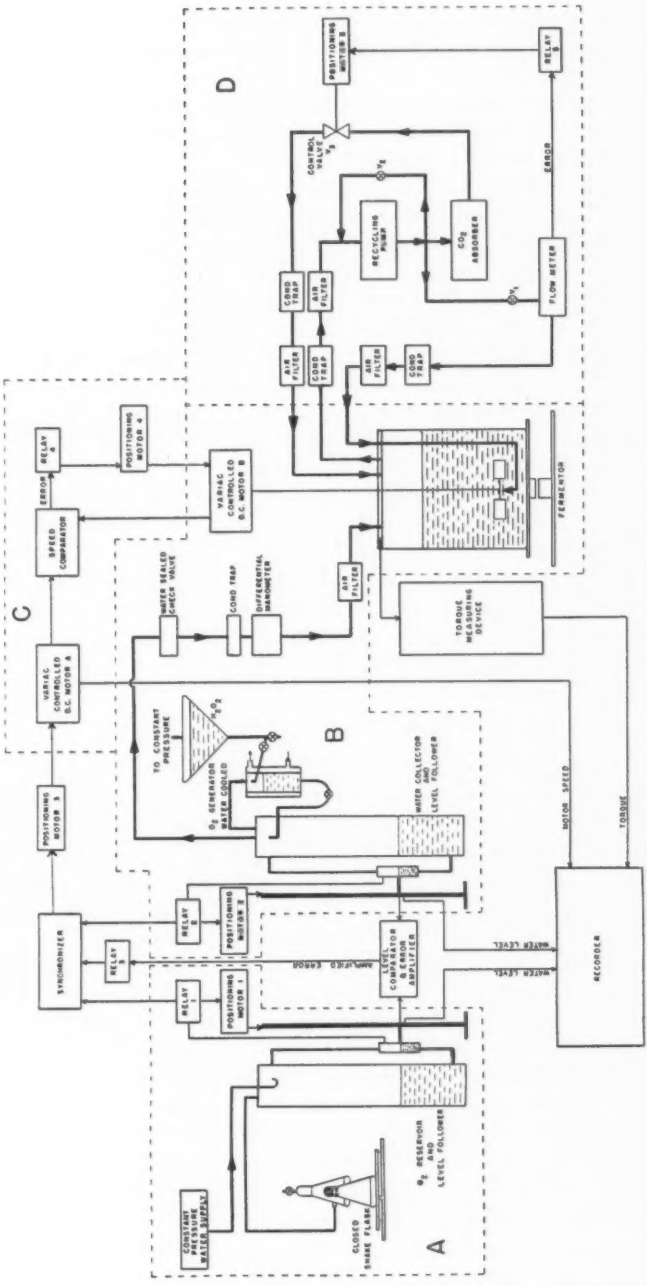

FIG. 1. Schematic diagram of the aeration data translation system.

During a fermentation, the oxygen consumed by the organisms upsets the pressure equilibrium between the fermentor and the gas spaces of water collector and oxygen generator. An equivalent amount of hydrogen peroxide is hence drawn in to compensate for the quantity of oxygen utilized. The concentration of hydrogen peroxide is selected to compensate for the difference in volume between fermentor and shake flask.

As the water levels in both the oxygen reservoir and the water collector cylinders rise, their rates of rising are compared from time to time with the help of a level comparator. The difference is amplified mechanically to operate relay 3, which with the help of a positioning motor 3[3] turns the variac speed control dial of motor *A* in such a direction that it changes the stirring speed to nullify the difference. A synchronizing timer switch is used to close the circuit between relay 3 and positioning motor 3 for a preset length of time after either one of the level follower bulbs makes a move. The speed of motor *A* is coupled to that of the stirring motor *B* through a speed comparator and a relay which operates the positioning motor 4 for the speed control dial of the stirring motor (block *C*). This arrangement eliminates the effect of the load disturbances on the stirring speed. The latter responds only to the command of the set speed of the motor *A*. Thus, the speed of stirring in the fermentor is indirectly regulated by the relative rates of the level rise in the cylinders. Changes in the stirring speed alter the oxygen uptake rate of the organism in the fermentor. This rate is then expressed in terms of the rate of rise of the level in the water collector cylinder. This closed loop regulating system makes it possible for the consumption of hydrogen peroxide by the tank fermentor to follow the oxygen uptake in the shake flask.

Level Comparator and Error Amplifier

It may be seen in Fig. 2 that the device to compare water levels in the reservoirs and amplify their differences is simply a lever system. The extension of the platform which carries the level follower bulb of the water collector supplies the fulcrum for the lever arm *C*. The latter is hinged to the platform which carries the follower bulb of the oxygen reservoir. A plastic idler bar *B* which has whisker and main contacts is hinged to the fulcrum rod and presses against a friction board with a sponge rubber pad in between. This makes it possible for the idler bar to stay where it is left. The lever arm is made of a brass bar with a $\frac{1}{4}$ in. slot cut at the end. The amplification factor is about 3. The main contact of the idler bar is placed in the slot. As one of the level follower bulbs makes a move, the slot end of the lever bar makes an amplified motion. If the amplitude of the motion is beyond the limit of the slot, the lever bar will touch the main contact of the idler bar and push the latter to a new position. The whisker contact only touches the lever bar when the idler bar assumes a lower position. The lever bar is electrically connected to contact *B*, while the main and whisker contacts are connected to contacts *A* and *C* respectively, of the electronic circuit (Fig. 5) which operates the positioning

[3]*One revolution per minute Bodine K.Y.C. 22 motor, a product of Bodine Electric Co., Chicago, Ill.*

motor 3. The connections are made such that when the idler bar assumes lower position the positioning motor turns the variac dial to increase the stirring speed and vice versa.

The variac dial is turned by the positioning motor 3 with friction drive. The ratio of the diameter of the friction disks is 1: 17. The diameter of the

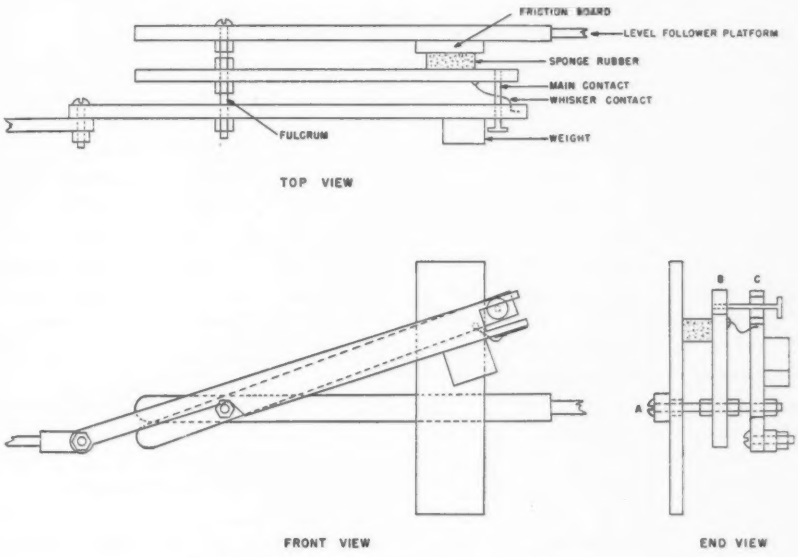

FIG. 2. Level comparator and error amplifier.

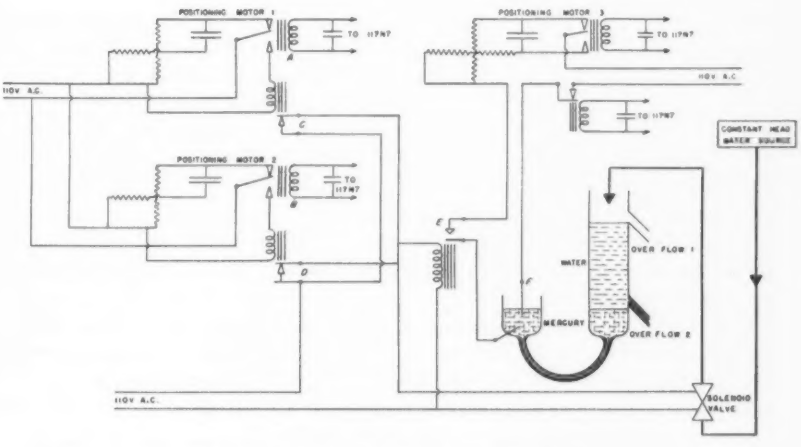

FIG. 3. Synchronized contact time limiter.

variac dial disk is 8.5 in. A 36 gage nichrome wire wound around the edge of the dial disk and a stationary sliding contact serve as a potentiometer to record the position of the dial. A current passing through the potentiometer is so adjusted that the potential drop across the entire wire is 9.7 mv. Since motor *A* carries only a small constant load, the motor speed can be expressed in terms of the dial position.

Synchronized Contact Time Limiter

When the idler bar assumes a new position the positioning motor will turn until one of the level followers moves to disengage the relay contact. Since the time interval between two successive movements of the level follower bulbs varies widely with the rate of oxygen uptake, this inevitably creates oscillations of high amplitude. This variation is minimized by insertion of a switch which permits current to flow to the positioning motor for a desired period after either or both of the follower bulbs make a move. This sequential process is performed by a set of relay arrangements shown in Fig. 3. As mentioned previously, the positioning motor relay circuits for the level followers move the bulbs only in the upward direction as the water levels rise in the cylinders. The other contacts of the single pole double throw relays *A* and *B* are available to operate normally closed a-c. relays *C* and *D*.

The circuit closure of either or both of these relays (*C* and *D*) energizes another normally closed a-c. relay *E*, and at the same time opens a solenoid valve to fill up the timer cylinder with water, thus closing the circuit at *F*. The relay contact *E* and the mercury contact *F* are connected in series to the power line of the positioning motor 3.

As the positioning motor 1 and/or 2 ceases to move, both the relays *C* and *D* become energized, the contact *E* is closed and likewise the solenoid valve. The contact *F* remains closed until water in the timer cylinder drains through the overflow 2 to its breaking point.

The over-all effect of this arrangement is that the positioning motor 3 alters the stirring speed only when the main contact of the level comparator, the relay contact *E*, and the mercury contact *F* make simultaneously closed circuit. This can occur only after the level follower bulb makes a move.

Motor Speed Comparator

The load on the stirring motor often varies as the physical consistency of the fermenting broth changes and causes variations in stirring speed. These may be nullified by standardizing the speed of the motor continuously against that of another motor running with a small load. This is done by the speed comparator as shown in Fig. 4.

The speed comparator consists of a plexiglass disk *A*, and a brass disk *B* (each 3 in. diameter). Disk *A* is driven by a variable speed d-c. motor *A*[4] after a speed reduction with a gear of 1:800 ratio. Disk *B* is driven by the d-c. stirrer motor *B*[5], with a gear reduction of 1:75. These two disks are mounted

[4]*Variable speed motor 2T60, purchased from Gerald K. Heller Co., Baltimore, Maryland.*
[5]*1/15 h.p., variac speed control motor, purchased from General Radio Co., Cambridge, Mass.*

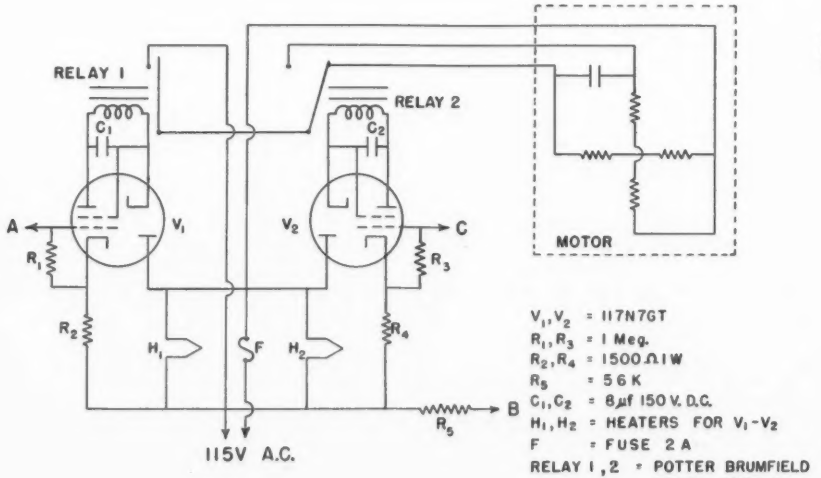

FIG. 5. Circuit diagram for the relay and positioning motors 3 and 4.

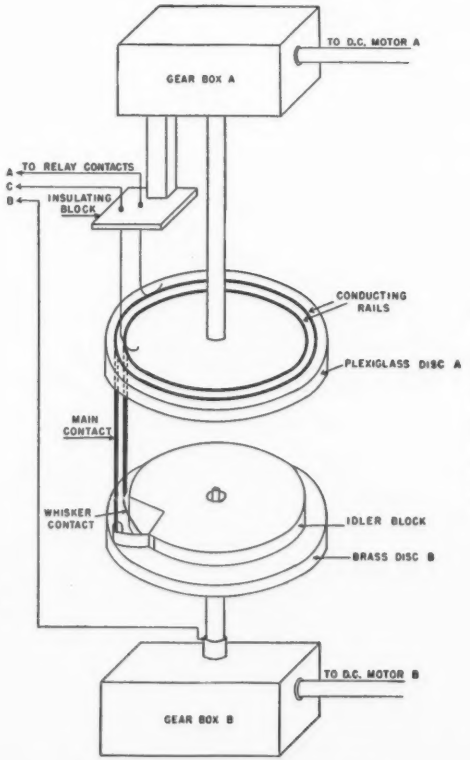

FIG. 4. Motor speed comparator.

concentrically and turn in the same direction. An idler brass disk ($\frac{1}{4}$ in. thick and 2.5 in. in diameter) with a contact slot on the side is placed concentrically on disk *B*, and is free to slide. Disk *B* is connected to terminal *B* of the relay-motor circuit (see Fig. 5). Disk *A* is furnished with main and whisker electrical contacts which are connected to terminals *A* and *C* of the relay-motor circuit through platinum rails and sliding contacts on the disk. The main contact is placed in the slot of the idler block. When disk *A* rotates faster than *B*, both the main and the whisker contacts are in touch with the idler block and activate positioning motor 4 to increase the speed of stirring motor *B*. When the reverse is true, only the main contact touches the idler disk and the positioning motor reduces the stirring speed. Thus, the speed of the motor *A* controls that of the stirring motor.

The coupling between the positioning motor and the variac dial of stirring motor is also made with friction disks. To slow down the dial movement, a diameter ratio of 1:8.5 was used. The circuit diagram for the relays and positioning motors 3 and 4 is shown in Fig. 5. It may be seen that the make and break of terminals *C* and *B* (whisker contact) reverses the direction of the motor while that of the terminals *A* and *B* (main contact) switches on and off the power line.

Air Flow Regulator

During a fermentation, because of changes in stirring speed and increases in suspended matter, there is an appreciable variation in resistance to air flow through the medium. The resistance variation in air flow is automatically corrected with the regulator system shown in Figs. 6 and 7. This regulator is, in effect, a capillary flowmeter with a double arm on one side of the capillary and a single arm on the other side. The inner walls of these arms are coated with water repellent Desicote.[6] Nichrome electrodes are adjusted to give the desired flow rate. They are electrically connected to the contact terminals *A*, *B*, and *C* of the relay-positioning motor circuit (Fig. 5). When changes in the rate of air flow exceed a previously set limit, the flowmeter fluid in the arms will make a contact for electrode *B* with electrode *A* in the single arm or with electrodes *A* and *C* in the double arm. This activates positioning motor 5 to turn the air flow control valve V_3 in such a direction that it nullifies the effect of the disturbance. Air flow is regulated by squeezing the rubber tubing against a wall *B* (Fig. 7). The bolt *C* (28 threads per inch) is mounted through a threaded collar *D* which is turned in a bearing mounted on a stationary plate at a rate of $\frac{1}{3}$ r.p.m. by a 1 r.p.m. positioning motor coupled through a gear system G_1 and G_2. With the rectangular bolt-head *A* pressing against guide plate *E*, the bolt moves back and forth without turning when the threaded collar rotates in one direction or the other. The range of this motion is limited by a microswitch pressing against bolt head *A*.

Fermentor and Torque Recording Device

The fermentor, a glass jar (8 liter), is similar to that described by Rivette *et al.* (8) except that the agitator is a four-bladed turbine impeller and the

[6]*A product of Beckman Instrument Inc., South Pasadena, Calif.*

FIG. 6

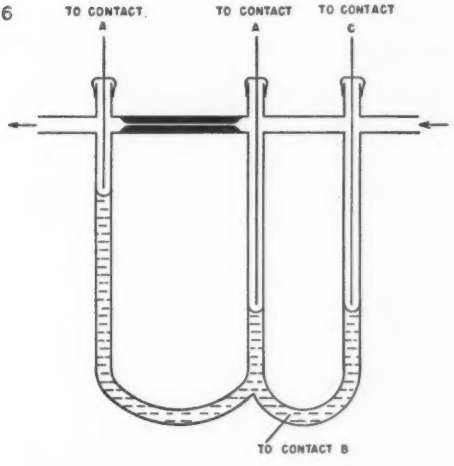

FIG. 7

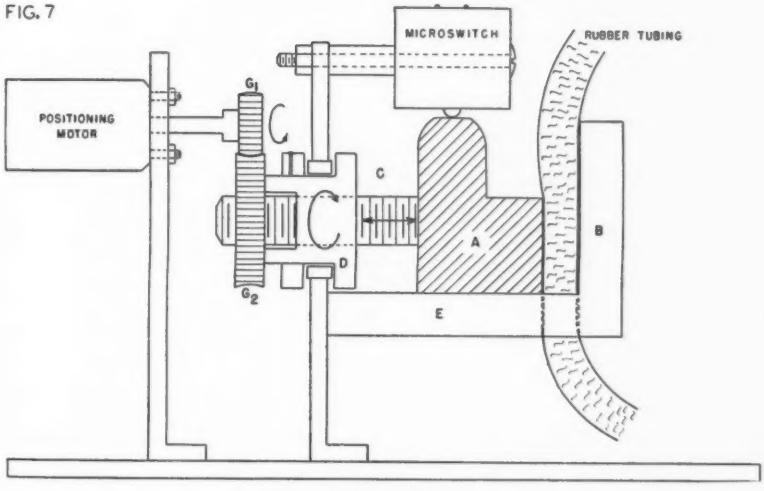

FIG. 6. Air flow regulator.
FIG. 7. Air flow control valve.

bearing for the stirring shaft is mounted on a shelf above the fermentor (Fig. 8). The entry of the shaft to the fermentor is doubly sealed with mercury and lard oil. All tube connections to the fermentor are made with flexible 3/16 in. I.D. rubber tubing and are placed close to the center of the jar top.

The torque measuring device (Fig. 9) is similar to that described by Cooper *et al.* (3) except that the counter weight is a piece of uniform steel rod (9 in. long and 0.75 in. in diameter), with added weight on the top, immersed in a pool of mercury. The length of rod above the mercury surface represents the

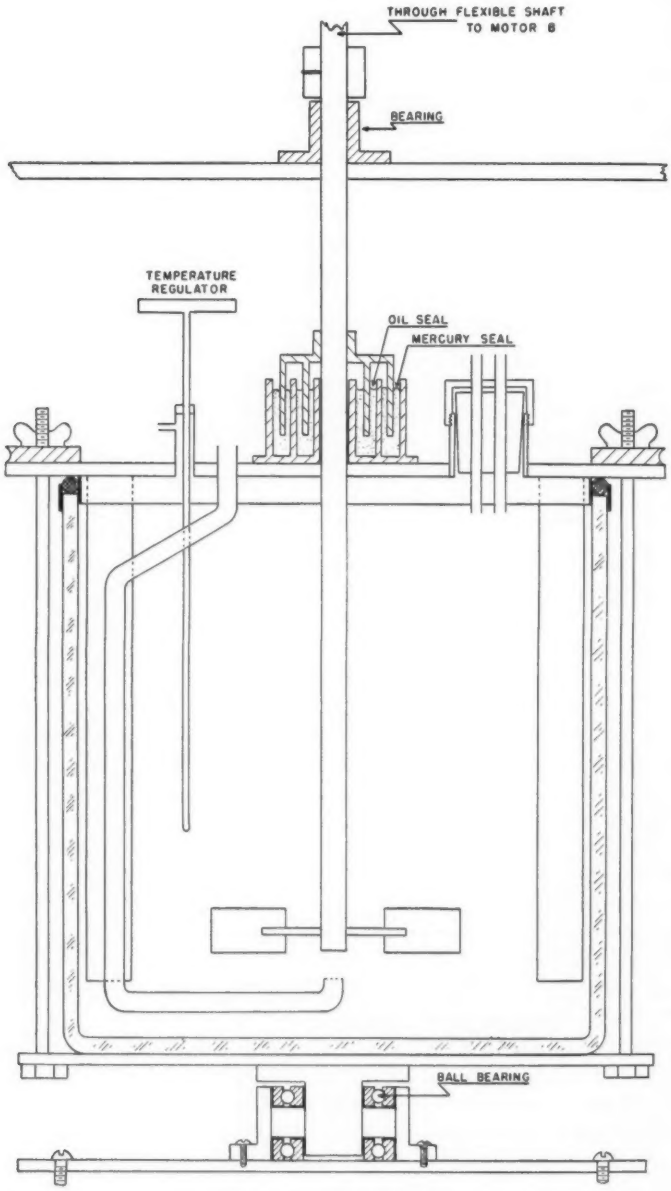

FIG. 8. Stirred tank fermentor.

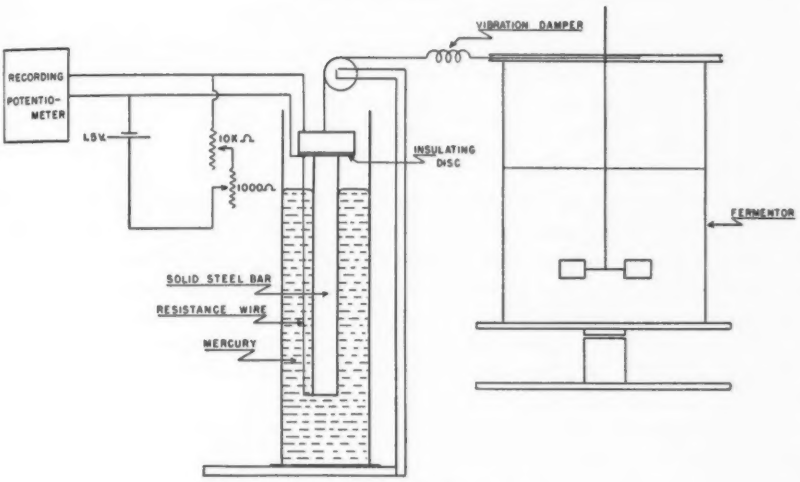

FIG. 9. Torque recording device.

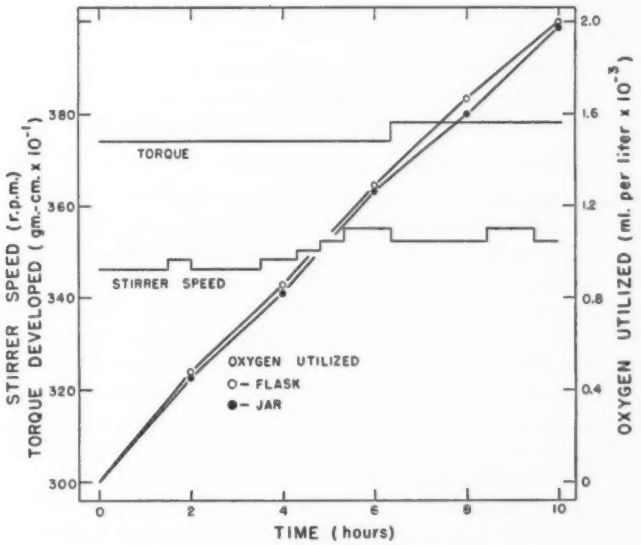

FIG. 10. Stability of the translation system.

magnitude of counter weight required. The change in the extent of immersion is measured and recorded as the potential drop across a nichrome wire (28 ohms per foot) stretched along the side of the rod. Both wire and mercury must be kept clean.

EXPERIMENTAL AND RESULTS

The performance of this device was tested by fermentation of glucose with *Ustilago zeae* PRL 1306 and production of α-amylase with *Aspergillus niger* PRL 558. Both the stability and the reproducibility of the apparatus were studied.

Stability and Reproducibility

With the present arrangement, oscillation of the stirrer speed may be reduced during the period of steady fermentation by decreasing the contact time of the synchronized contact time limiter. However, a decrease in contact time would hamper the ability of the fermentor to respond to fast changes of the rate of oxygen uptake in the shake flask. Furthermore, since the relation between the control dial position of motor *A* and the stirrer speed is non-linear, the effect of contact time to the stirrer speed oscillation also varies with the stirrer speed. Thus, the choice of a proper contact time is essential.

With the present control elements, a contact time of five seconds was found satisfactory for fermentations requiring stirring speeds higher than 300 r.p.m. during the steady fermentation period.

Data summarized in Fig. 10 shows the stability of stirring speed and torque developed during a steady oxygen uptake period of *U. zeae* fermentation. The stirrer speed oscillation was about 10 r.p.m. and the change in torque was insignificant.

The reproducibility of the device was tested with the sulphite oxidation method at two levels of aeration. For a given aeration rate, the stirring speed may be reproduced within the range of the stable oscillation.

Glucose Fermentation by Ustilago zeae PRL 1306

Preliminary runs showed that the initial lag of the fermentation in the shake flask was less than that in the fermentor. It was not possible for the uptake of oxygen in the fermentor to follow that in the flask even at high rates of stirring. Therefore, a culture grown for 24 hr. was used for the coupled fermentation.

The medium of Thorn and Haskins (12) was used. The flask (500 ml.) contained 100 ml. medium and was incubated on a New Brunswick Shaker[7] (320 r.p.m.) at 26.5° C. The fermentor contained 4 liters of medium, and a solution containing 11.8% hydrogen peroxide was employed as the oxygen source. Consumption of one volume of this solution by 4 liters of medium is equivalent to the utilization of the same volume of gaseous oxygen per 100 ml. of medium under these conditions. The initial speed of stirring was set at about 100 r.p.m. to ensure that the culture was in suspension. The fermentor was kept at 25.5° C. in a water bath. The rates at which air was recycled through the medium and sodium hydroxide scrubber were adjusted to 1 liter per minute.

The results of this fermentation are summarized in Fig. 11. When the system reached a steady state the stirring speed remained between 325 and 350 r.p.m. to duplicate the rate of oxygen uptake in the shake flask (average 200 ml. per

[7]*A product of New Brunswick Scientific Co., New Brunswick, N.J.*

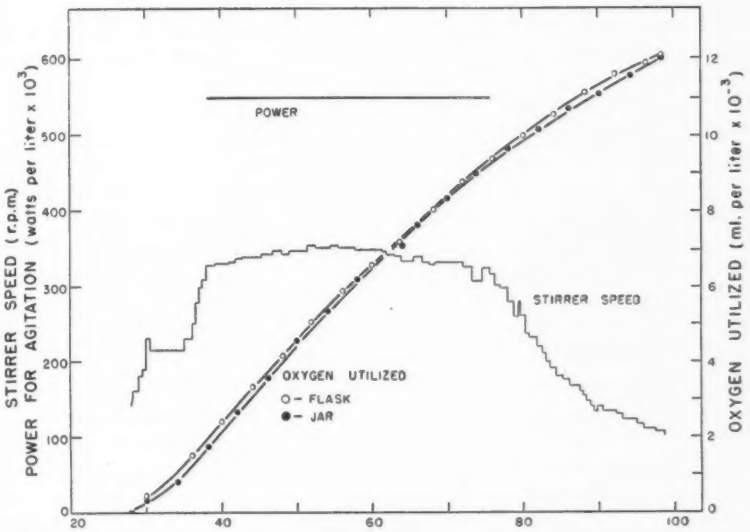

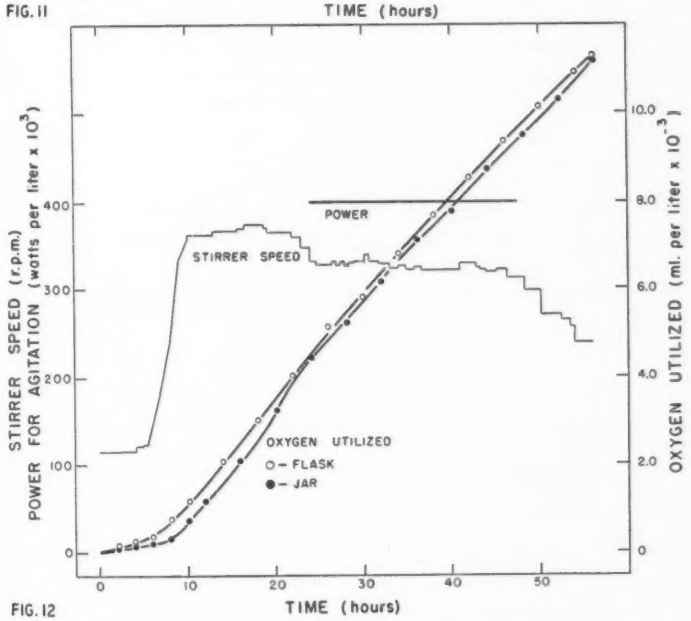

FIG. 11. Translation of aeration data from shake flask to stirred tank for *U. zeae* fermentation.

FIG. 12. Translation of aeration data from shake flask to stirred tank for *A. niger* fermentation.

liter per hour). During this period, little change in torque occurred and the variation of stirring power was caused mainly by changes in stirring speed. An average of 0.55 w. per liter of medium was required by the stirrer.

α-Amylases Production by Aspergillus niger PRL 558

A medium containing 1.0% yeast extract, 2.0% starch, 0.5% calcium carbonate, salts (11), and 5% inoculum was fermented in the same manner as that for *U. zeae* except that the shaker speed was set at 260 r.p.m. and the fermentors were coupled at the beginning of the fermentation.

The results are summarized in Fig. 12. The longer initial lag phase in the fermentor caused a considerable amount of overshooting of the stirring speed. However, a steady state was reached later. During this period the stirring speed varied between 310 and 340 r.p.m. and the rate of oxygen uptake was 200 ml. per liter per hour. The average power required to maintain such an aeration was 0.4 w. per liter of medium. The α-amylase and cell yields obtained from the tank were comparable to those obtained from the shake flask.

These results show that the oxygen uptake in a shake flask may be duplicated in a stirred tank with the help of the present translation device, and the corresponding aeration conditions for the stirred tank may be determined. One should be reminded that the master fermentor may be of any type, but the slave fermentor has to be of agitated type and its magnitude of aeration may be delicately controlled. Because of the limiting nature of the oxygen supply system, this device is only suitable for smaller fermentors with which extensive aeration studies are made.

ACKNOWLEDGMENT

The author wishes to express his appreciation to Messrs. M. Anderson, P. F. Baines, and W. Hogg for the construction of the fermentor, electronic relays, and glass parts of the apparatus.

The technical assistance of Mr. A. Funk is also gratefully acknowledged.

REFERENCES

1. Bartholomew, W. H., Karow, E. O., Sfat, M. R., and Wilhelm, R. H. Ind. Eng. Chem. 42: 1801. 1950.
2. Chain, E. B., Paladino, S., Callow, D. S., Ugolini, F., and Van Der Sluis, J. Bull. World Health Organization, 6: 73. 1952.
3. Cooper, C. M., Fernstrom, G. A., and Miller, S. A. Ind. Eng. Chem. 36: 504. 1944.
4. Hixson, A. W. and Gaden, E. L., Jr. Ind. Eng. Chem. 42: 1792. 1950.
5. Hoover, S. R., Jasewicz, L., and Porges, N. Instrument and Automation, 27: 774. 1954.
6. Karow, E. O., Bartholomew, W. H., and Sfat, M. R. Agriculture and Food Chem. 1: 302. 1953.
7. Masterson, S., Peers, C. H., and Willows, R. Brit. Patent No. 672,860. May 28, 1952.
8. Rivett, R. W., Johnson, M. J., and Peterson, W. H. Ind. Eng. Chem. 42: 188. 1950.
9. Saeman, J. F., Locke, E. G., and Dickerman, G. K. FIAT Final Rept. 499. 1945.
10. Shu, P. Agriculture and Food Chem. 1: 1119. 1953.
11. Shu, P. and Blackwood, A. C. Can. J. Botany, 29: 113. 1951.
12. Thorn, J. A. and Haskins, R. H. Can. J. Botany, 29: 403. 1951.
13. Wegrich, O. G. and Shurter, R. A., Jr. Ind. Eng. Chem. 45: 1153. 1953.
14. Wise, W. S. J. Gen. Microbiol. 5: 167. 1951.

THE STORAGE AND TRANSFER OF LOW POTENTIAL HEAT

I. GLAUBER'S SALT AS A HEAT STORAGE MATERIAL[1]

By J. W. Hodgins and T. W. Hoffman

ABSTRACT

A study has been made of the variables affecting the storage of low potential heat as the heat of fusion of Glauber's salt. The geometry of the container was determined as the result of preliminary experiments, using a moving transfer surface. Extensive experiments with the final design yielded the following information:

(*a*) Low over-all efficiency is the result of segregation of phases as crystal growth proceeds.

(*b*) Short heat paths in the exchanger are essential to keep thermal resistance at a minimum.

(*c*) The crystal growth rate in this system is the rate governing process once phase isolation has occurred.

(*d*) Over-all heat transfer coefficients are in the order of 2 B.t.u./hr. (sq. ft.) (° F.).

INTRODUCTION

The utilization of solar energy for domestic heating resolves itself into three separate problems: the collection of heat from the sun, the storage of the heat until required, and the employment of the stored heat for keeping a dwelling at a suitable temperature.

The first of these problems has been exhaustively investigated by Hottel and others at the Massachusetts Institute of Technology (1) and Lof and associates at the University of Denver (2). The collector panel design, which represents a compromise between ideal performance and reasonable economy, in general consists of two or more glass plates separated by an air gap, with a black metal absorbing surface receiving the energy transmitted through the glass, which also reduces back radiation. The heat is removed from the black plate by a transfer fluid, usually air, and absorbed in the storage unit before the air is recycled to the panel. The optimum angle of tilt for collection of winter solar energy at the latitude of Kingston (44° 14′ north) is 62° from the horizontal facing due south, which will provide for 12% better operation than will a vertical panel (3).

The storage of the heat collected by the panel is, of course, of supreme importance to any solar heating system. The present investigation is an attempt to elucidate some of the controlling variables involved in the storage of low potential heat, and its transfer on demand.

Although the transfer of heat from a panel to a storage unit will be efficient if the collector temperature is kept high, the efficiency of the acceptance of solar energy will diminish with rising plate temperature. Thus, if the efficiency

[1]*Manuscript received April 1, 1955.*

Contribution from Department of Chemical Engineering, Royal Military College of Canada, Kingston, Ontario. The material in this paper constitutes work done in partial fulfillment of the requirements for an M.Sc. degree from Queen's University (T.W.H.). A paper on this investigation was presented at the Chemical Engineering Conference in Ottawa, March, 1955.

of the collection step is to be kept to a reasonable figure, it has been found necessary to maintain the collector plate below 120° F., which enables collection to be made of early morning and late afternoon radiation. In order to keep construction costs within reason, and because of low night temperatures, air has been chosen as the heat transfer medium, despite its low transfer coefficients. The storage unit must accept heat from the air at 120° F. and must transfer it to a dwelling area which is about 70° F.

Heat storage capacity can be provided in two ways—as heat capacity or as heat of fusion. Heat of fusion storage has already been used in this connection (5), but no detailed study has been made which will permit of the best design of a storage–transfer unit. The principal advantage of storing heat by chemicals is the saving in space—for example Glauber's salt ($Na_2SO_4 \cdot 10H_2O$) will store nearly five times as much heat as an equal volume of water between 80–120° F. Ice itself is the best storage material because it has the highest heat of fusion per unit weight or volume. However, because the melting point is not within the comfort range, a higher melting material must be used. The limitations on the storage material are fairly severe; it must be cheap to be practical, and it must have a melting and freezing point between 100° F. and 85° F. The substances which best fulfill these criteria are crystalline hydrates, whose heat of fusion is higher, the greater the proportion of water of hydration in the molecule.

All of the salts considered as heat storage materials undercool to a marked extent, and therefore nucleating material must be found which has the following requisites.

(*a*) It will act as a seeding material—that is, it must be nearly isomorphic with the hydrate used.

(*b*) It must be only sparingly soluble in the solution resulting from the melting of the crystal. Any significant solubility of course lowers the melting point.

(*c*) It must survive its environment through repeated cycles of melting and crystallization.

In a heat storage apparatus, crystallization will start on the heat transfer surface where the nucleating material is present—that is, on the bottom surface in a stationary system where the nucleating agent is denser than the hydrate. The resulting crystal mantle will then present resistance to the flow of heat and to convection in the exchanger. In this investigation a study has been made of the effect of container geometry, agitation, and rate of heat withdrawal upon the operation of heat storage equipment with a view to providing design criteria for a full-size unit. All of the experiments were done using Glauber's salt as the storage material, since a satisfactory nucleating agent was already at hand (6). It melts at about 90° F. with a heat of fusion of 104 B.t.u. per pound, and can be purchased for about $9.00 per ton.

Dr. Maria Telkes has found that borax ($Na_2B_4O_7 \cdot 10H_2O$) is a satisfactory nucleating agent to induce crystallization of Glauber's salt (6). At 90° F. the solubility is 2.71 gm. per 100 gm. of saturated sodium sulphate solution (4), at which concentration the phase transition temperature is lowered by about

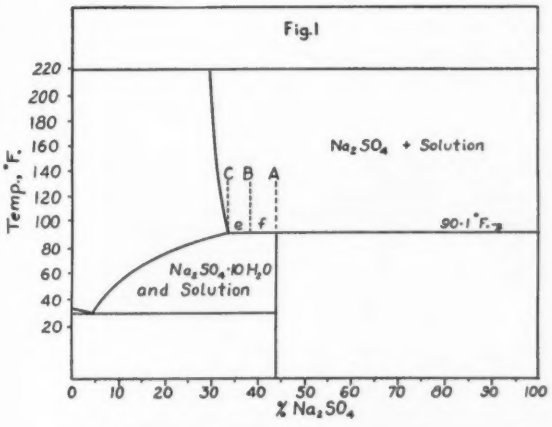

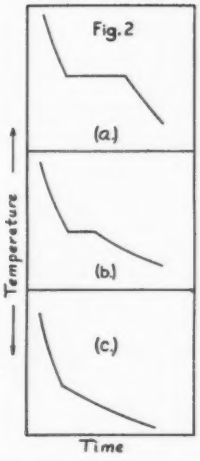

FIG. 1. Phase equilibrium diagram for the system sodium sulphate – water.
FIG. 2. Time–temperature cooling curves.

2.5° F. In order to discuss the experimental results, it is appropriate at this point to examine the phase equilibrium diagram for the system sodium sulphate – water (Fig. 1), and to consider the effects of cooling a system with concentrations of *A*, *B*, and *C* respectively. It is important to keep in mind that these considerations apply only to equilibrium conditions.

Point *A* in Fig. 1 represents a system having the stoichiometric composition of Glauber's salt, but at a temperature above the melting point of the hydrate. Because of the incongruent melting point, there is a considerable proportion of solid anhydrous Na_2SO_4 present—a proportion which increases with rising temperature. Because of its high density, it rests on the bottom of the container. If one cools the mixture at *A*, constantly maintaining equilibrium conditions, the hydrated salt begins to crystallize at 90.3° F., and the temperature remains constant until the entire melt has gone solid, with the composition $Na_2SO_4 \cdot 10H_2O$. The time–temperature cooling curve is represented schematically in Fig. 2 (*a*). If the same cooling operation be performed on a mixture of composition *B*, the temperature halt at the phase transition temperature will be shorter, and at equilibrium, the two phases will consist of Glauber's salt and a solution saturated with respect to Glauber's salt, in the relative amounts e: f (Fig. 1). Further heat liberation will be possible only on lowering the temperature below 90.3° F. The cooling curve for this mixture is illustrated in Fig. 2 (*b*). Cooling of the saturated solution (composition *A*, Fig. 1), will not give any plateau at 90.3° F., and heat liberation will result only in continual lowering of the temperature. Its typical cooling curve is illustrated in Fig. 2 (*c*). Therefore, maximum heat at the highest possible steady temperature is available when sodium sulphate and water are present in the stoichiometric ratio of 1: 10.

EXPERIMENTAL PROCEDURE

The experiments were done in two stages. The first apparatus was designed to illustrate the efficiency of moving the heat transfer surface with respect to the crystal mass, in order to shed the crystal mantle which forms. This apparatus (illustrated in Fig. 3), consisted of a rotating coil in the crystal mass, (Glauber's salt and 4 wt.-% of $Na_2B_4O_7 \cdot 10H_2O$) carrying water which re-

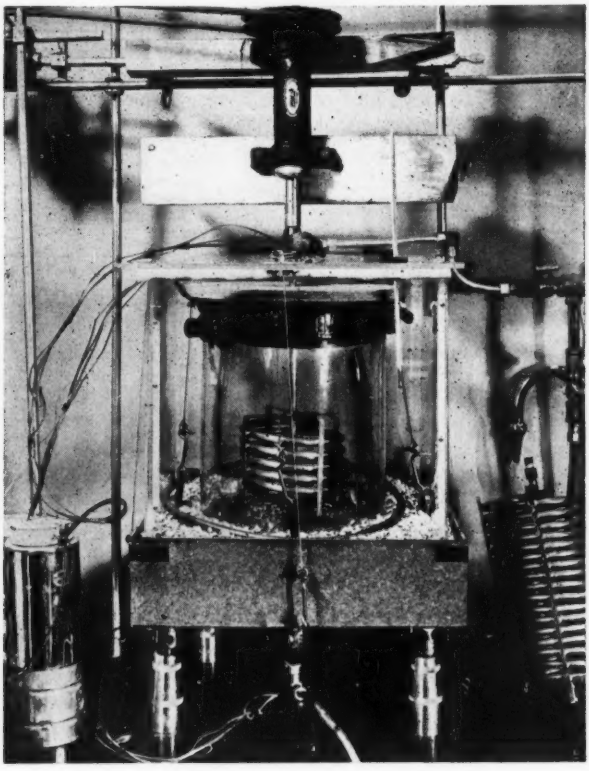

FIG. 3. Rotating coil storage–transfer unit.

moved the heat. An insulating Lucite box surrounding the jar containing the crystals was kept at the same temperature as the salt, thus permitting observation without heat transfer through the container walls. The Glauber's salt was first melted by hot water passed through the coil, and when the temperature of the mixture reached a suitable point, heat withdrawal was begun by cool water passed through the rotating coil. Temperatures of the water stream and of the salt mass were read on copper–constantan thermocouples.

The second apparatus, built as a result of the experience with the first, had an entirely different form. In this exchanger, the salt was contained in a

shallow copper tray, 24 × 6 × 1 in., with air ducts of the same dimensions above and below the tray. With the exception of the tray itself, all of the components of this apparatus were thermal insulators—the outer walls of the ducts were made of asbestos board, and the entire apparatus encased in Foamglas insulation. The apparatus is illustrated in Fig. 4. Air, metered by a rotameter *A*, passed through a heating tube *B* into the exchanger. The first

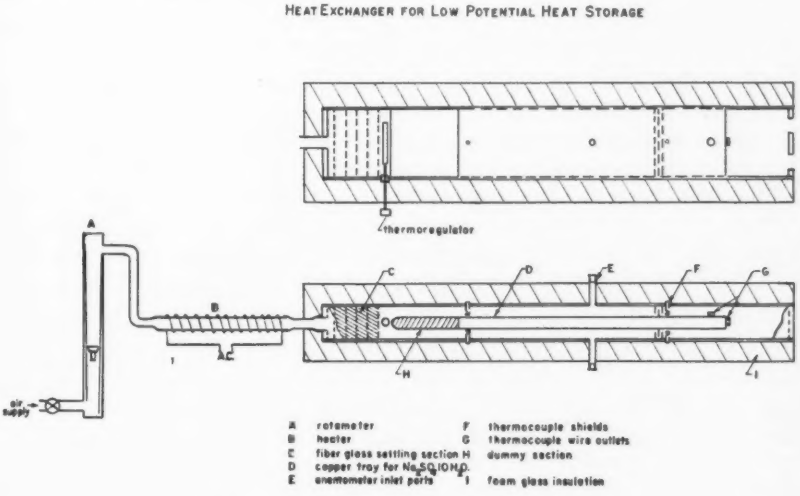

FIG. 4. Shallow tray storage–transfer unit.

four inches of the chamber were packed with sheets of glass wool air filter material to provide a calming section. Ahead of the copper tray a dummy section of insulating board (*H*) protruded six inches in front of the copper tray, to ensure stable boundary layer formation at the exchanger surfaces. Thus the tray section simulates the center portion of a practical heat exchanger. Air temperatures were measured by shielded copper–constantan thermocouples, constantly monitored on automatic recording potentiometers. Since most of the air flowrates were in the streamline or transition region, it was necessary to use a three-pass baffle mixer just ahead of the air outlet thermocouple. This caused impingement of the air on the copper sheet, and thus an increase in the transfer at that point. This spurious effect was minimized by a cemented asbestos sheet at the location of the impinging air. Altogether, 39 thermocouples were used to measure air and plate temperatures and gradients in the solution. A calibrated hot wire anemometer was used to measure the air flow in the ducts, thus providing assurance that the mass flowrate of the air was the same in each duct. As in the first apparatus, the salt was first melted at an air temperature controlled by the thermoregulator, and heat was then withdrawn from the tray by cool air passed on either side. Here too, the filling was Glauber's salt and 4 wt.-% of $Na_2B_4O_7 \cdot 10H_2O$.

RESULTS AND DISCUSSION

In the first apparatus, crystallization started, as one would expect, upon the heat transfer surface of the rotating coil. Movement of the surface with respect to the saturated solution did nothing to remove the crystal mantle. Crystallization also occurred at the bottom of the container, and as the crystals grew, the hard crystal mass soon prevented coil rotation. The crystals in the bottom were obviously of two kinds—the hydrated crystals formed an impervious blanket over the anhydrous salt, thus stopping any subsequent hydration reaction. From this experiment the following conclusions were drawn:

(i) Stratification of the nucleating agent does not seem to be a serious deterrent to crystallization.

(ii) Crystallization occurs on the heat transfer surface, and the crystals are not detached by movement of the solution past this surface.

(iii) The heat exchanger must be designed without internally moving parts.

(iv) The hard crystal structure precludes the use of large tank-like containers, because of the difficulty of transferring heat to melt the crystal mass.

(v) The container must be shallow, so that the heat paths are short.

All of the quantitative data were obtained using the second apparatus (Fig. 4). A typical experiment is illustrated by the time–temperature cooling curves shown in Fig. 5, in which an air flowrate of 12.6 c.f.m. (Re = 2300) was used. The flowrate was chosen as the result of considerations of the probable dimensions of a practical storage unit, and the heat requirement of 50,000 B.t.u. per hour—a normal value for a medium-sized dwelling in the locality of Kingston. The solution temperatures shown represent a portion of the solution which is unaffected by the impingement effect. The bottom plate temperatures at various locations are shown as the run proceeds. The undercooling amounted to 6.3° F., at which time crystallization began. There is no appreciable plateau at the maximum, and the solution temperature quickly reaches a lower limit of 81° to 82° F. Air at lower temperatures than this will be useless for space heating.

Heat was automatically turned on when the air temperatures reached 82° F., and the heating of the tray began. A short temperature plateau was observed, followed by a sharp rise; the melting point is markedly higher than the highest temperature reached during heat extraction. At any particular time, the quantity of heat transferred is

$$dq = W.\ Cp.\ d\theta.\ (T_{out} - T_{in}), \text{ where}$$

Cp = specific heat of the air, B.t.u./lb. (°F.).
$d\theta$ = time interval, hr.
W = flowrate, in lb./hr.

By integrating under the time–temperature curves, the total heat transferred over a given period was calculated; from these measurements, the total heat-in was found to equal the total heat-out, and this heat balance indicates negligible heat loss in the exchanger. Over the crystallization period, 94 B.t.u. of heat were realized, as compared with the total theoretical amount of heat

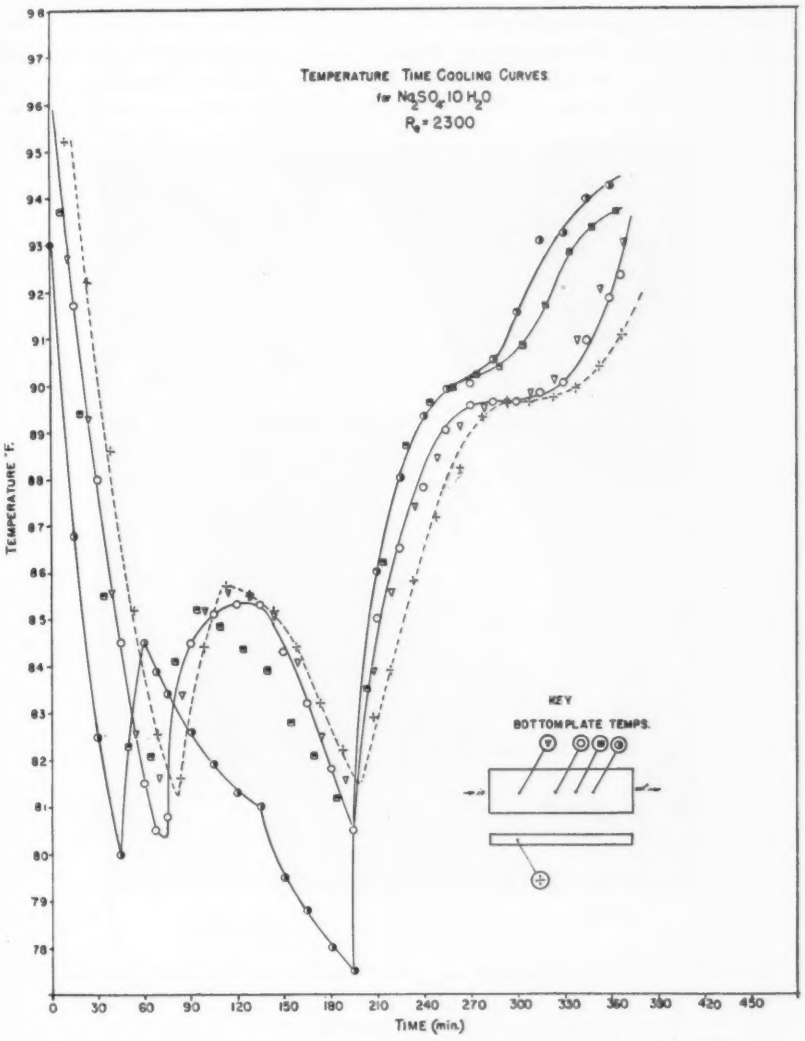

FIG. 5. Time–temperature cooling curves for tray exchanger containing Glauber's salt.

capable of being stored in the test section, 570 B.t.u. This same efficiency of 16.5% was obtained over the range of air flows used—from Re 1000 to Re 2300.

In Fig. 6 is shown a piece of crystal taken from the exchanger after the runs were complete, which illustrates the two phases, anhydrous sodium sulphate, surmounted by Glauber's salt. The hydrated salt so effectively isolates the anhydrous layer from the solution that the supernatant liquid never crystallizes. Because of the inverse solubility of the anhydrous salt (it becomes less

soluble with rising temperature), the crystals form a very dense cake on repeated cycling of temperature. That is, on heating, additional anhydrous material deposits in all the crevices, while on cooling these deposits are only slightly dissolved before the isolating hydrate mantle forms.

FIG. 6. Crystal formation from tray heat exchanger.

Once the blanket of $Na_2SO_4 \cdot 10H_2O$ has isolated the anhydrous salt, the system acts as a saturated solution, which explains the absence of a long plateau in the cooling curve. Further crystallization will occur only as a result of lowering the temperature. Since rate of crystallization is a function of the degree of undercooling, equilibrium conditions do not prevail once this isolation is complete, and the temperature attained is then a function of the rate of withdrawal and the inherent crystal growth rate.

The 16.5% efficiency observed in these experiments represents the worst efficiency. In practical use the withdrawal of heat would be intermittent, and during the off cycle the equilibrium conditions would be at least partially regained. Nonetheless, it would still behave as a saturated solution, for no reaction with the anhydrous salt on the bottom is possible.

Fig. 7 illustrates the variation with time of the total heat transferred and the over-all heat transfer coefficient. The large heat transfer at the beginning of the cooling and heating runs represents the heat capacity of the apparatus. The minimum in the cooling run denotes the beginning of heat generation and the decreasing of internal thermal gradients. As the plate temperature increases, the over-all heat transferred from the bottom plate reaches a maximum, while the over-all heat transfer coefficients remain fairly constant, decreasing only slightly as the salt builds up on the bottom. Since there is no

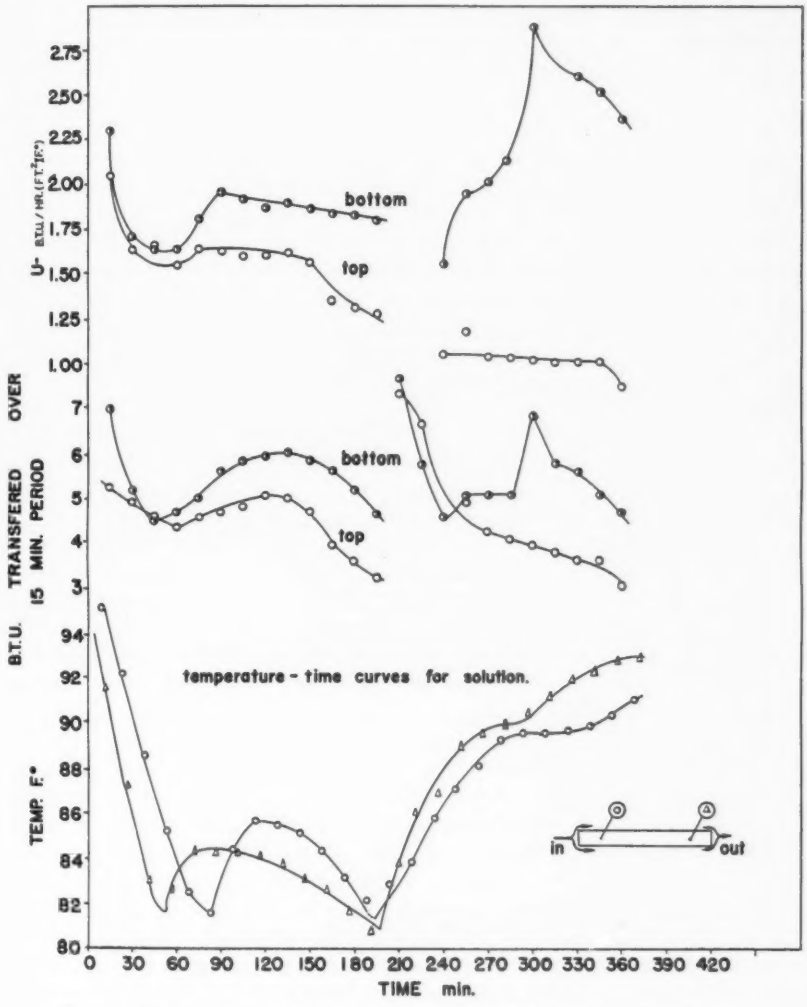

FIG. 7. Heat transfer coefficients and heat transferred in tray heat exchanger.

crystal growth on the top plate, heat reaches it only by convection and conduction through the liquid, resulting in a lower heat transfer. Because the nucleating agent is denser than its environment, crystallization starts at the worst possible place—at the top of the insulating layer of anhydrous sodium sulphate.

On the heating cycle, the total heat transferred and the heat transfer coefficient for the bottom plate reach a sharp maximum. This maximum represents the point where the internal surface contact changes from solid to liquid, allowing for better heat acceptance. Heat transferred through the top plate is low, for it is removed from the plate by conduction through the liquid. The plate reaches a high temperature quickly, and therefore high internal temperature gradients are set up.

CONCLUSION

Although Glauber's salt has been used in an actual heating installation (5), the present investigation has indicated that it is not a very satisfactory storage material. The manner in which equilibrium is hindered by the growth of the hydrate to isolate the anhydrous salt lowers the efficiency at the outset; and the fact that crystal growth from the saturated solution cannot keep up with the rate of heat abstraction means that the slow step in the heat removal cycle is governed by the inherent crystal growth rate. Other more promising systems are under current investigation. The features being sought are homogeneity above the melting point, ease and reproducibility of nucleation, and rapidity of crystal growth.

ACKNOWLEDGMENT

The authors are glad of this opportunity to acknowledge the co-operation and assistance of Dr. A. C. Plewes, of the Department of Chemical Engineering of Queen's University.

REFERENCES

1. HOTTEL, H. C. and WOERTZ, B. B. Trans. ASME. 64: 91–104. 1942.
2. IRISH, E. R. and LOF, G. O. G. A paper delivered to the Symposium on Space Heating with Solar Energy, Mass. Inst. Technol. 1950.
3. JORDAN, R. C. and THRELKELD, J. L. Heating, Piping, and Air Conditioning. 25: 111–122. December, 1953.
4. SBORGI, U., BOVALINE, E., and CAPELINE, L. Gazz. chim. ital. 54: 298–321. 1924.
5. TELKES, M. Heating and Ventilating, 46: 79–86. November, 1949.
6. TELKES, M. Ind. Eng. Chem. 44: 1308–1310. 1952.

NOTE

AN OPERATION-TIME CONTROLLER FOR A RECORDING POTENTIOMETER[1]

By G. O. Handegord and D. G. Cole

Certain applications of recording potentiometers require that a record be made for only part of each day. In some cases, such as solar radiation measurements, the "on" period of the recorder does not coincide with normal working hours and manual starting and stopping of the instrument is not possible. The instrument can be operated continuously but this results in an excessive amount of chart being used, particularly in the winter months when sunshine occurs for only eight hours.

A standard time switch, such as the "Inter-matic" Model TS-60SP, manufactured by the International Register Co., may be employed to stop and start the instrument at any predetermined time. This time switch is commonly used in business places to operate display lighting during the dark hours of the evening.

When the potentiometer used incorporates a standard cell circuit with automatic standardization, one difficulty arises in that the time switch may stop the instrument when the standardizing circuit is closed, resulting in an undesirable drain on the standard cell during the "off" period. This difficulty may be overcome by incorporating a micro switch in parallel with the time switch to operate the instrument should the time switch open while standardization is in progress.

The Brown 153XIIV-X-27, strip chart recording potentiometer used for solar radiation measurements in Saskatoon has been modified in the above manner. The time switch and micro switch are incorporated into the instrument as shown in Fig. 1. The micro switch employed is a normally open type #BZ-2R, installed so that its contact pin bears against the standardization slide wire mechanism. During standardization, the mechanism is moved in towards the chassis so that the micro switch pin protrudes fully, thus closing the switch and operating the instrument until standardization is complete. The micro switch is mounted on a brass plate which is secured to one of the mounting posts of the standardization assembly cover as shown in Fig. 2. Both the time switch and micro switch are wired in parallel with the drive switch as shown in Fig. 3. This wiring arrangement does not involve any change in the original wiring of the instrument and all the connections may be made to the terminal board on the rear of the chassis.

The time switch and micro switch operate only the chart drive circuit of the instrument, power being supplied continuously during both "on" and "off" periods to the amplifier circuit as recommended by the manufacturer. Intermittent operation of the recorder as determined by the setting of the time

[1]*Issued as N.R.C. No. 3631.*

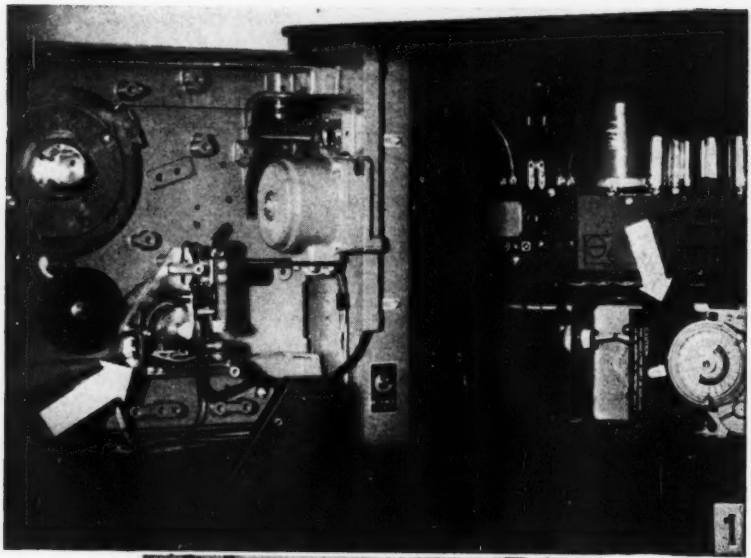

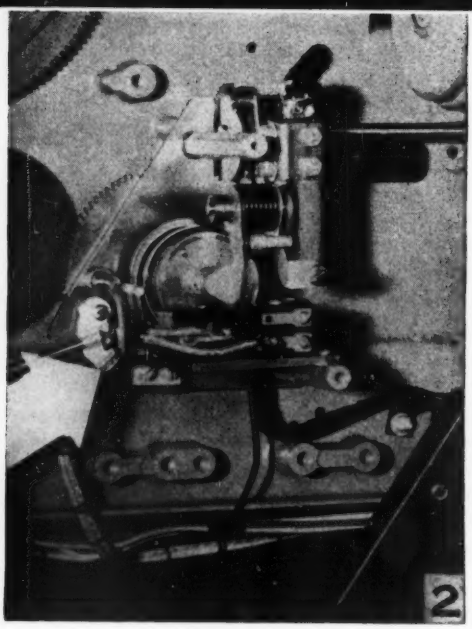

FIG. 1. Location of time switch and micro switch in recorder case.
FIG. 2. Close-up view of micro switch and mounting bracket.

switch is achieved with the instrument chart drive switch in the "off" position. Continuous operation of the recorder is readily obtained by moving the chart drive switch to the "on" position.

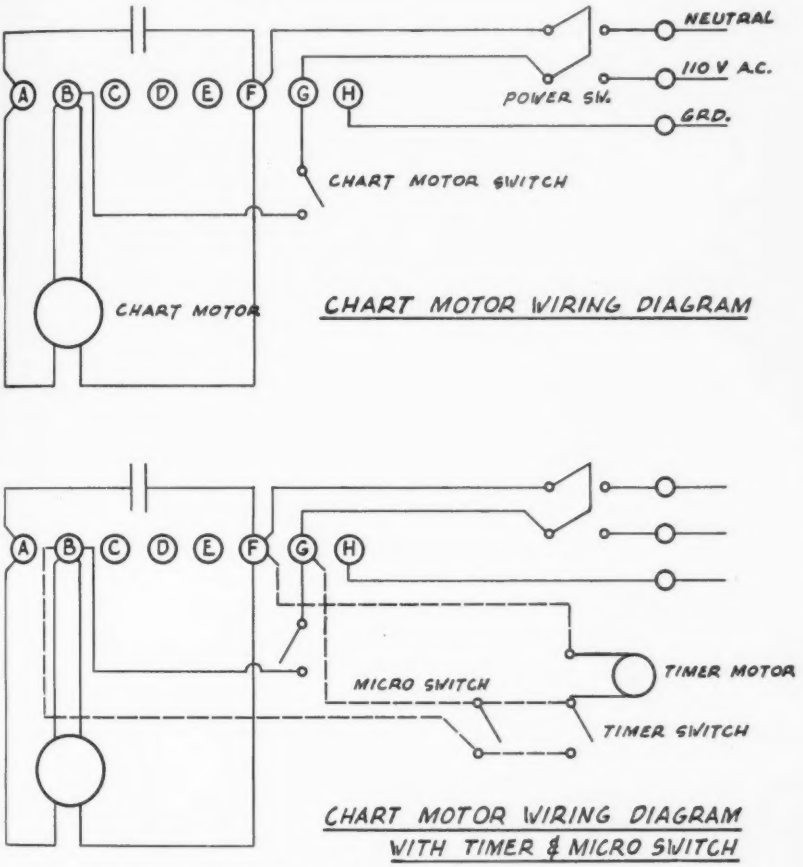

FIG. 3. Chart motor wiring diagram.

The total cost of materials required for this automatic switching arrangement is approximately thirteen dollars. The savings involved in chart consumption for the particular application cited will be approximately eighteen dollars per year, based on an average period of 14 hr. of sunshine and a chart cost of four dollars per roll.

RECEIVED APRIL 14, 1955.
PRAIRIE REGIONAL STATION,
DIVISION OF BUILDING RESEARCH,
NATIONAL RESEARCH COUNCIL,
SASKATOON, CANADA.